Oligodendrocyte dynamics dictate individual performance outcomes of working memory training in mice

Takahiro Shimizu[1] *, Stuart G Nayar[1] *, Matthew Swire[1], Yi Jiang[1], Matthew Grist[1], David M Bannerman[2], Heidi Johansen-Berg[3], Katsutoshi Ogasawara[4], Koujiro Tohyama[5] and William D Richardson[1]

[1] Wolfson Institute for Biomedical Research, University College London, Gower Street, London WC1E 6BT

[2] Department of Experimental Psychology, University of Oxford, Oxford OX1 3TA

[3] Wellcome Centre for Integrative Neuroimaging, Department of Clinical Neurosciences, John Radcliffe Hospital, University of Oxford, Oxford OX3 9DU

[4] Technical Support Center for Life Science Research and [5]Department of Physiology – School of Dentistry, Iwate medical University, 1-1-1 Idaidori, Yahabacho, Shiwa-gun, Iwate 028-3694, Japan

* joint first authors

Correspondence to: William D Richardson w.richardson@ucl.ac.uk +44 (0)20 7679 6729

Key words: learning and memory, cognition, working memory training, mouse behaviour, T-maze, radial maze, rewarded alternation, adaptive myelination

Summary (125 words)

Motor skill learning stimulates and requires generation of myelinating oligodendrocytes (OLs) from their precursors. We asked whether OL production is also required for non-motor learning and cognition, using T-maze and radial arm maze tasks that tax spatial working memory. Maze training stimulated OL production in the medial prefrontal cortex, anterior corpus callosum (genu), hippocampus and fimbria; myelin sheath formation was also stimulated in the genu. Genetic blockade of OL differentiation and neo-myelination in *Myrf* conditional knockout mice strongly impaired training-induced improvements in maze performance. Remarkably, working memory performance of individual mice correlated closely with the scale of OL precursor proliferation and OL generation in their genu and anterior cingulate cortex during training, indicating a key role for adaptive OL genesis and myelination in cognitive processing.

Introduction

Oligodendrocytes (OLs), the myelin-forming cells of the central nervous system (CNS), are generated during development from OL precursors (OLPs), which arise in localized parts of the ventricular zones of the embryonic brain and spinal cord before proliferating and migrating widely to become almost uniformly distributed through the postnatal and adult CNS (Bergles and Richardson, 2015). Most myelinating OLs are formed in the early postnatal period (first ~6 postnatal weeks in mice) but OLPs continue to divide and generate new myelinating OLs throughout adulthood.

OLPs and newly-forming OLs can detect and respond to electrical activity in the axons that they contact. For example, OLPs express AMPA receptors, form physical synapses with axons and respond to glutamate released from active axons (Bergles et al., 2000; Kougioumtzidou et al., 2018). Neuronal activity stimulates OLP differentiation into OLs and/or survival of the new-forming OLs, thereby enhancing myelination of electrically active axons in preference to their inactive or less-active neighbours (Gibson et al., 2014; Mitew et al., 2015). Electrical activity or experience can also influence the number of myelin sheaths synthesized by individual OLs, or myelin sheath length or thickness (Mitew et al., 2015; Exteberria et al., 2016; Hughes et al., 2018; Swire et al., 2019; Bacmeister et al., 2022). These different sorts of modification alter the properties of neuronal circuits in response to physiological demand and are known collectively as “adaptive myelination”.

Adaptive myelination has been shown to be important for learning and memory. McKenzie et al. (2014) blocked formation of newly-forming OLs by conditional knockout (cKO) in OLPs (using *Pdgfra-CreER*^{T2}) of *Myelin regulatory factor* (*Myrf*), encoding a transcription factor that is necessary

for OL differentiation. The *Myrf*-cKO mice were impaired at learning a new motor skill – running at speed on a "complex wheel" with unevenly spaced rungs. When wild type mice learned to run on the complex wheel, OL differentiation and/or survival was stimulated as early as a few hours into learning (McKenzie et al., 2014; Xiao et al., 2016). Pan et al. (2020) and Steadman et al. (2020) used a similar *Myrf*-cKO approach (using *NG2-CreER*^{TM}) in contextual fear-conditioning paradigms and found that new OL production was required for formation and recall of long-term (28 day) fear memory, though not for fear learning per se or for short-term (24 hour) recall. In addition, Steadman et al. (2020) found that long-term spatial memory in the Morris water maze was impaired although, again, spatial learning per se and short-term recall were unaffected. Together, these studies suggest that new myelin is required to modify and stabilize task-relevant circuits, with short and longer-term behavioural consequences that might be context-dependent.

Motor skill learning engages motor cortex, basal ganglia, cerebellum and other brain regions but is independent of the hippocampus (Milner, et al., 1998). On the other hand, fear learning and spatial learning require cognitive function and rely on coordinated activity of the hippocampus and other brain regions, but do not rely on OL generation. We were therefore driven to ask whether there are examples of non-motor learning that do depend on OL genesis. We chose to investigate the role of OL genesis in cognition, in particular the improvement in cognitive performance that can accompany working memory training in mice. This choice was influenced by the fact that working memory training in humans induces microstructural changes in white matter tracts (Takeuchi et al., 2010), similar to motor skills learning (Scholz et al., 2009; Sampaio-Baptista et al., 2013) and consistent with a role for adaptive myelination.

Working memory is a short-term, limited capacity memory system that in humans is crucial for cognitive processes involved in decision making and reasoning (Cowan 2008; Baddeley, 2010; D'Esposito and Postle, 2015; Chai et al., 2018). Working memory engages the frontoparietal network, together with its long-range interconnections through the corpus callosum and other tracts. Spatial working memory tasks additionally engage hippocampal circuits including the fimbria-fornix (Olton and Papas, 1979; Spellman et al., 2015). Working memory capacity/ performance in a given task can be improved (trained) through reiterative practice both in humans (e.g. Dahlin et al., 2008; Klingberg, 2010; Guye and von Bastian 2017; Linares et al., 2018) and mice (Light et al., 2010), although how training modifies the underlying psychological processes and neural circuits is not known.

We investigated the role of OL genesis in the performance of mice in T-maze and 8-arm radial maze tests, using "win-shift" protocols that train and assess spatial working memory (Olton et al., 1978; Rawlins and Olton 1982; McHugh and Bannerman, 2010; Bannerman et al., 2014; Sasaki et

al., 2018). We found that *Myrf*-cKO mice were unable to improve their performance in either a delayed non-matching to position (DNMP) T-maze task (rewarded alternation) or an analogous radial arm maze task, relative to control littermates, which improved their performance steadily over the 8- or 9-day training period. During maze training, wild-type mice increased OLP proliferation and production of newly-differentiated OLs in the prefrontal cortex and hippocampal formation, especially long-range connecting axon tracts in the anterior corpus callosum (genu) and fimbria. By immunofluorescence light microscopy and electron microscopy we also obtained evidence that the number of myelin sheaths and associated nodes of Ranvier in the genu were increased during training. Hence, working memory training, like motor skills training, both stimulates and requires active OL generation and myelin formation.

Remarkably, we found that the performance of individual animals in the radial arm maze correlated closely with the rate of OLP division and the number of newly-generated OLs that appeared in the genu, ACC and PLC/ ILC during training. Our findings indicate that OL generation and neo-myelination strongly influence cognitive ability, by strengthening structural connectivity or coordinating activity within and among distributed brain regions involved in working memory operations.

Results

Adult oligodendrocyte generation is stimulated by, and required for, various learning and memory tasks including motor learning, long-term spatial memory and remote fear memory (McKenzie et al., 2014; Xiao et al., 2016; Pan et al., 2020; Steadman et al., 2020; Bacmeister et al., 2020; 2022). We asked whether oligodendrocyte generation is also required for learning paradigms that rely on working memory performance.

Active OL generation is required for working memory training in the T-maze

The T-maze rewarded alternation task (Methods and Supplementary Video 1) uses a delayed non-matching to position (DNMP) protocol to assess spatial working memory and training-induced improvement in working memory performance over the duration of the task (Deacon and Rawlins 2006). *Myrf*-cKO mice (n=28) and littermate controls (n=26) were placed on dietary restriction one week prior to the 3 days of habituation and 8 days of training/ testing in the T-maze (Methods and Fig. 1A). On day 1 of training, *Myrf*-cKO mice, which cannot generate new OLs post-tamoxifen administration (McKenzie et al., 2014), performed at near-chance levels (~50% success rate) and did not improve significantly during the 8 days of training (Fig. 1B). In contrast, control littermates started at chance levels but steadily improved over the next 8 days, reaching significant divergence from *Myrf*-cKOs on days 7 and 8 (Fig.1B). These results suggest that active generation of new OLs is required for training-based improvement (learning) in the rewarded alternation task.

OL generation is not required for simple left-right discrimination in the T-maze

Mice were also trained in a simple, appetitively-motivated left-right discrimination task using the same T-maze apparatus. This task, therefore, has the same sensorimotor and motivational demands as the spatial working memory task described above. In this test, the same goal-arm was baited with a food reward (dilute condensed milk) on each trial during the full 3 days of the experiment for each mouse. Mice were released into the start-arm and had to choose whether to turn left or right at the T-junction in order to obtain the reward. Those that chose the non-baited arm were recorded as having made a reference memory error. On day 4 the location of the rewarded goal-arm was switched so that the other arm was now always baited, requiring the mice to adapt and turn in the opposite direction than before. Left and right goal-arms were counterbalanced among mice of both genotypes. Both groups of mice successfully learned the task and then subsequently learned to reverse their choice of arm. The performances of control and *Myrf*-cKO groups were superimposable, both before and after the reversal of goal-arms (Supplementary Fig. S1A). Therefore, active OL generation is not required for left-right discrimination learning. This suggests that the spatial working memory deficit reported above was not due to impaired sensorimotor or motivational processes, or an inability to discriminate between the arms of the T-maze.

OL generation is not required for recognition memory

Mice were then assessed on two spontaneous, exploratory tasks of recognition memory - the novel object recognition task (NOR) and the object location task (OLT). There was no difference in the performance of *Myrf*-cKOs versus control littermates in the NOR, whether tested 10 min or 24 h after first encountering the objects (Supplementary Fig. S1B, C). There also was no difference between *Myrf*-cKOs and controls in the OLT after 10 min (Supplementary Fig. S1D, E). Thus, active OL generation is not required for spatial or object recognition memory. Taken together, these data indicate that *Myrf*-cKO mice can learn to recognize either objects or locations as familiar.

We also tested *Myrf*-cKO mice in the open field test for 10 min (Methods). There were no significant differences in mean speeds, distances travelled, or trajectories in bird nest and heat maps (Supplementary Fig. S1F-H). Therefore, *Myrf*-cKO mice are not hypo- or hyper-active compared to controls.

OL generation is required for working memory training in the 8-arm radial maze

To test the generality of the spatial working memory deficit that we observed on the T-maze, in a more complex spatial environment with increased memory demands, we also assessed

experimentally naïve mice on an 8-arm radial maze (RAM) task, which requires mice to visit 4 assigned arms sequentially during forced runs before then selecting the 4 unvisited arms from all 8 possible options during the free run phase of the task.

Our RAM protocol consisted of 6 days habituation followed by 9 days of training/ testing (Methods and Fig. 1A). During days 1-4 of training the control mice (n=29) and *Myrf*-cKOs (n=28) both improved their performance at a similar rate and reached a similar level of performance, assessed either by success rate or percent of "perfect trials" (Methods and Fig. 1C, D). After day 5 of training, the control group out-performed the *Myrf*-cKOs, performing significantly better than the *Myrf*-cKOs by success rate on each of days 5 to 9 (e.g. day 8: controls 76.7% ± 2.6%, *Myrf*-cKOs 64.6% ± 2.1%, p=0.006, Šídák's post-test) (Fig. 1C). The proportion of "perfect trials" achieved by controls also exceeded that of the *Myrf*-cKOs on each of days 5 to 9 (e.g. day 8: controls 32.8% ± 6.1%, *Myrf*-cKOs 9.5% ± 4.0%, p=0.0001) (Fig. 1D). The proportion of perfect scores over all 9 testing days was also significantly higher in the control group (9.4% ± 1.8% versus 3.5% ± 1.0%, p=0.004). The average running speed of *Myrf*-cKO mice over the 9 days of RAM training was the same as controls (Supplementary Fig. S1I).

There are at least two strategies that mice can adopt during the free run phase of the RAM task: 1) they can use working memory to identify unvisited arms and collect the remaining rewards directly, or 2) they can visit all arms sequentially, clockwise or anti-clockwise, until they collect all the rewards ("daisy-chaining"). This latter approach, which does not tax working memory, was used by the majority of mice, both *Myrf*-cKOs and controls, during the first few days of the task (Supplementary Videos 2-4). A proportion of mice subsequently switched to the more efficient working memory-based approach (Supplementary Video 2). By manual modelling we determined that the average score that can be achieved over many trials by daisy-chaining is independent of whether mice run clockwise or anti-clockwise and ranges between 53% and 56% (mean, 55%) for the 4-arm forced run patterns that we employed (see Methods). This is close to the starting score we observed on day 1 for both *Myrf*-cKOs and controls, consistent with both groups initially using the daisy-chain strategy (Fig. 1C). However, the final average scores attained on days 8 and 9 by the control group (77% and 78% respectively) cannot be achieved by daisy-chaining and must rely on working memory. This is also suggested by the rapidity of correct goal-arm selection in the latter stages of training (Supplementary Video 2). Note that daisy-chaining can never result in a "perfect trial" with the 4-arm patterns that we employed. Therefore, our RAM data (Fig. 1C, D) strongly imply that *Myrf*-cKO mice cannot train their working memory to the same degree as normal controls and that de novo OL generation is a critical factor in training-induced working memory improvement.

There was no evidence that the spatial working memory deficit in *Myrf-cKO* mice was due to an increased susceptibility to proactive interference. We re-plotted the data of Fig. 1C, separating the first 3 trials from the last 3 trials of each day (Supplementary Fig. S1J). The choice accuracy of control mice was not different between the earlier or later trials of each day, nor was the choice accuracy of *Myrf*-cKOs. This suggests that *Myrf*-cKO mice were no more likely than their control littermates to confuse arm visits made in their current trial with visits made in previous trials, so this was not a factor in the under-performance of *Myrf*-cKOs in the RAM.

Working memory training stimulates new OL generation in the anterior corpus callosum

Motor skill learning is known to stimulate OLP proliferation and OL generation so we asked whether the same is true of working memory training. To label and visualize newly-generated OLs we administered EdU to phenotypically wild type mice (mixed background from the *Myrf*-cKO breeding colony, without tamoxifen) via their drinking water (0.2 mg/ml) during 9 days of training in the radial arm maze task (Fig. 1A). A control group remained in their home cages throughout (home-cage controls). OL lineage cells were analyzed either 1- or 14-days post-training, by immunolabelling for Pdgfra (to visualize OLPs) or with monoclonal CC1 (to visualize differentiated OLs) together with EdU labelling to detect recently-divided, newly-generated cells (Fig. 2).

Working memory engages the medial prefrontal cortex (mPFC), including the anterior cingulate cortex (ACC) and prelimbic/ infralimbic cortex (PLC/ ILC), as well as their inter-hemispheric connections in the anterior-most corpus callosum (CC, also known as the genu). Spatial working memory also involves the hippocampal formation including CA1 and the fimbria (Fim). Therefore, we analyzed OLP proliferation and differentiation into OLs in these different brain regions of "good-performing", "poor-performing" and home-cage control mice. Good-performers were mice that achieved ≥10 perfect trials during the 9 days of training, poor-performers ≤5 perfect trials. Poor-performers experienced the same handling and exposure to the RAM as good-performers but performed less well; they therefore provided an ideal control group for separating genuine learning effects of RAM-training from potentially confounding effects of differing experience and activity. Data for anterior CC and ACC are shown in Fig. 3 and Supplementary Table 1; data for PLC/ ILC, hippocampal CA1 and fimbria (Fim) are shown in Supplementary Fig. S2 and Supplementary Table 2.

Proliferation of OLPs was dramatically increased (~4-fold) in good-performers compared to either poor-performers or home-cage controls in the anterior corpus callosum, judging by the number-density of EdU^+ $Pdgfra^+$ cells at 1-day post-RAM training (Fig. 3B). As a result, the population density of $Pdgfra^+$ OLPs was also significantly increased in good-performers at 1-day post-RAM (Fig. 3C). The number-density of EdU^+, $CC1^+$ newly-differentiated OLs was also significantly

increased at 1-day post-RAM in good-performers compared to poor-performers or home-cage controls (Fig. 3D; statistics in Supplementary Table 1). Because of when EdU was administered, stimulation of OLP proliferation must have occurred during the 9 days of RAM working memory training.

By 14-days post-RAM training, the number-density of EdU$^+$ Pdgfra$^+$ OLPs in good-performers had dropped to a similar level as in poor-performers or home cage controls (Fig. 3E). This likely reflects differentiation of a fraction of recently-divided OLPs into EdU$^+$ CC1$^+$ OLs, because the number-density of EdU$^+$ OLs at 14-days post-RAM is similar to the number of EdU$^+$ OLPs at 1-day post-RAM, while the number of EdU$^+$ OLPs drops to near baseline (compare Figs. 3B, E, G). Somewhat unexpectedly, the overall population density of Pdgfra$^+$ OLPs in good-performers remained elevated at 14-days post-RAM (Fig. 3C, F) despite the number of newly-divided EdU$^+$ Pdgfra$^+$ OLPs having fallen to baseline. Presumably, Pdgfra$^+$ OLPs continued to divide and accumulate after the RAM training period, when EdU was no longer available. Whether, over the longer term, all these excess EdU-negative OLPs eventually differentiate into OLs and return the OLP population density to pre-training levels is an intriguing question.

We observed similar effects of RAM-training on OL lineage dynamics in the fimbria, a white matter tract that connects the hippocampus to its major output regions and is required for spatial aspects of learning (Dahmani et al., 2020) including spatial working memory (but not reference memory) (Olton and Papas, 1979). Here too, RAM-training stimulated OLP proliferation leading to an increased number of EdU$^+$ Pdgfra$^+$ OLPs at 1-day post-RAM in good-performers relative to controls, and an elevated number of newly-formed EdU$^+$ CC1$^+$ OLs that persisted until at least 14-days post-RAM (Supplementary Fig. S2; statistics in Supplementary Table 2).

Almost no EdU$^+$ CC1$^+$ OLs were formed in the corpus callosum of *Myrf*-cKOs that had undergone RAM training (Fig. 3D, G), as expected (McKenzie et al., 2014; Pan et al., 2020; Steadman et al., 2020).

RAM training stimulates OLP proliferation and OL genesis in the prefrontal cortex

In control mice, the steady-state population density of Pdgfra$^+$ OLPs in the gray matter of the ACC is similar to that in the underlying white matter (Fig. 3C, F, I, L) but the rate of OLP proliferation and EdU incorporation is around ten-fold less in gray than in white matter (Fig. 3B, E, H, K). Nevertheless, at 1-day post-training, EdU incorporation into Pdgfra$^+$ OLPs in the ACC was strongly increased (~2- to 7-fold) in good-performers relative to poor-performers or home cage controls (Fig. 3H). This proliferative response also results in an increase in the population density of Pdgfra$^+$ OLPs in good-performers (Fig. 3I) and an increase in production of newly-differentiated

EdU^+ $CC1^+$ OLs (Fig. 3J) at 1-day post-RAM. However, these increases are temporary and short-lived in the ACC; by 14-days post-RAM there were no longer any detectable differences among groups, except for a non-significant trend towards an increase in newly-formed $CC1^+$ OLs in good-performers (Fig. 3K-M; statistics in Supplementary Table 1).

Very similar short-term effects of RAM-training on OL population dynamics were observed in another part of the medial PFC, the PLC/ ILC (Supplementary Fig. S2). In hippocampal CA1 there might have been a transient training-induced stimulation of OLP proliferation at 1-day post-RAM but no evidence of increased OL differentiation (Supplementary Fig. S2); however, there were low numbers of OL lineage cells in hippocampal CA1, reducing confidence in this conclusion.

As in the CC, OL generation was practically non-existent in the cortical gray matter of *Myrf*-cKO mice (Fig. 3J, M; Supplementary Fig. S2D, G), as expected.

Working memory performance is proportional to the scale of OLP proliferation and differentiation
It was striking that good-performing mice generated many more new OLs, on average, than their poor-performing counterparts. It was also noticeable that there was generally a wider spread of data points among the good-performers than among the poor-performing mice (e.g. Fig. 3C, D) — raising the possibility that, even among the good-performers, different behavioural outcomes of RAM training might reflect different levels of training-induced OLP proliferation and differentiation. We tested this by plotting the number of "perfect scores" achieved by individual mice (both good- and poor-performers) against the numbers of newly-divided EdU^+ $Pdgfra^+$ OLPs and new EdU^+ $CC1^+$ OLs present in different brain regions post-training. Data for the anterior CC and ACC are shown in Fig. 4 and for PLC/ILC, CA1 and fimbria in Supplementary Fig. S3 (statistics in Supplementary Table 3). Strikingly, at 1-day post-RAM in the anterior CC there was a strong correlation between the RAM performance of individual mice and the numbers of EdU^+ $Pdgfra^+$ recently-divided OLPs ($R^2 = 0.84$), the overall population density of $Pdgfra^+$ OLPs ($R^2 = 0.46$) and the number of EdU^+ $CC1^+$ newly-generated OLs ($R^2 = 0.61$) (Fig. 4A-C).

In another white matter tract, the fimbria, there was also a high correlation at 1-day post-RAM between working memory performance and the number-density of EdU^+ $Pdgfra^+$ recently-divided OLPs ($R^2 = 0.76$) but no significant correlations with either $Pdgfra^+$ OLP population density ($R^2 = 0.14$) or density of EdU^+ $CC1^+$ newly-formed OLs ($R^2 = 0.28$) (Supplementary Fig. S3G-I and Supplementary Table 3).

In the ACC at 1-day post-RAM we found strong correlations between individual RAM performance and number of EdU^+ $Pdgfra^+$ OLPs ($R^2 = 0.72$) and $Pdgfra^+$ OLP population density ($R^2 = 0.53$)

(Fig. 4D, E). However, there was no correlation between RAM performance and number of EdU^+ $CC1^+$ newly-generated OLs (R^2 = 0.21) (Fig. 4F). Similar high correlations between working memory performance and density of EdU^+ $Pdgfra^+$ proliferating OLPs were observed in the PLC/ILC and hippocampal CA1 (R^2>0.7 in both regions) (Supplementary Fig. S3A, D and Supplementary Table 3).

By 14-days post-RAM the correlations between behavioural performance and the number density of OL lineage cells in all regions examined were no longer significant, or much reduced in significance (data not shown).

Training-induced myelination of axons in the anterior corpus callosum

The marked and persistent increase in numbers of newly-generated OLs in task-relevant white matter tracts (anterior corpus callosum and fimbria) in good-performing RAM-trained mice raised the question of whether these new OLs formed additional myelin sheaths. Additional myelin sheaths are necessarily accompanied by extra nodes of Ranvier and paranodal loops, so we asked whether the number-density of node/paranode structures increased in the corpus callosum (CC) following successful RAM training. We immunolabelled sections of CC for voltage-gated sodium channel 1.6 ($Na_V1.6$, present in the axonal membrane at nodes) and the adhesion molecule Caspr (in the axonal membrane under the paranodal myelin membrane loops) (Fig. 5A). We counted node/paranode structures in coronal sections through the anterior CC, which carries transverse connections between left and right ACC, of good-performing RAM-trained mice and home cage controls. This analysis suggested that there might be an increase in the density of nodal structures – hence myelin sheaths – in RAM-trained mice, although this did not reach statistical significance [control, 6.44 ± 0.36 nodes/100 μm^2, n=7 mice; RAM-trained, 7.48 ± 0.36 nodes/100 μm^2, n=7 mice, p =0.066, t =2.03, df =12 (unpaired Student's 2-tailed t-test)] (Fig. 5B). We also measured the lengths of nodes and paranodes in these immunolabelled sections and found that, at this level of analysis, there was no detectable change in the average lengths of nodes, paranodes or complete node/paranode structure in RAM-trained mice versus home-cage controls (Fig. 5C-E). [Nodes: control, 1.69 ± 0.20 μm, n=780 from 4 mice; RAM-trained, 1.51 ± 0.11 μm, n=737 from 4 mice, p=0.44, t=0.82, df=6. Paranodes: control, 1.57 ± 0.05 μm, n=1106 from 4 mice; RAM-trained, 1.47 ± 0.03 μm, n=1084 from 4 mice, p=0.17, t=1.6, df=6. Complete nodal structures: control, 4.79 ± 0.27 μm, n=534 from 4 mice; RAM-trained, 4.47 ± 0.06 μm, n=542 from 4 mice, p=0.32, t=1.1, df=6 (unpaired Student's 2-tailed t-tests)]

The distribution of nodal structures was non-uniform in the CC (Fig. 5A) suggesting that sampling variation might obscure otherwise significant effects. We therefore turned to electron microscopy (EM), hoping for more reproducible selection of target areas, especially in the anterior-posterior

dimension. Back-scatter EM from the surfaces of parasagittal sections mounted on glass microscope slides (Methods) allowed us to observe and image large uninterrupted areas of tissue. We counted all end-on profiles of myelin internodes, nodes and paranodes in ~50 μm-wide strips spanning the full ~300 μm dorsal-ventral extent of the CC, 600-650 μm from its anterior tip (Fig. 5F, G). We compared good-performing RAM-trained mice with home cage controls in this experiment so as to more easily match sample sizes, and since we had previously found no differences between numbers of new OLs induced by RAM-training in poor-performers versus home cage controls (Fig. 3). We found that there was no significant change in the numbers of myelinated axon profiles in good-performing RAM-trained mice versus controls (good performers: 125 ± 6 /mm^2, 14,231 myelinated axon profiles counted from n=6 mice; home cage: 113 ± 6 /mm^2, 12,871 myelinated axons from n=6 mice, unpaired Student's 2-tailed t-test p=0.16, t=1.4, df=10) (Fig. 5H), accompanied by a significant ~25% increase in the number of node/paranode profiles (good performers: 6.1 ± 0.33 /mm^2, 689 nodes/paranodes counted from n=6 mice; home cage: 4.8 ± 0.29 /mm^2, 545 nodes/paranodes from n=6 mice, unpaired Student's 2-tailed t-test p=0.016, t=2.9, df=10) (Fig. 5I), consistent with an increase in the number of discrete myelin internodes. This indicates that the new training-induced EdU$^+$ CC1$^+$ OLs form new myelin sheaths – although we cannot rule out that pre-existing OLs are partly (or wholly) responsible for the additional myelin internodes. In RAM-trained animals the ratio of node/paranode profiles to all myelinated axon profiles ("node+paranode frequency") was also increased (good performer: 4.8% ± 0.15%, n=6; home cage: 4.3% ± 0.22%, n=6, unpaired Student's 2-tailed t-test p=0.050, t=2.2, df=10) (Fig. 5J), suggesting that the extra myelin sheaths might be shorter than the majority, on average, in keeping with those extra sheaths being newly-formed. The alternative interpretation, that nodes/paranodes might be longer, on average, in RAM-trained versus control mice, was ruled out by direct measurement of nodal structures (previous paragraph, Fig. 5C-E).

The apparent fractional increase in internode density in RAM-trained mice versus controls, estimated by counting side-on views of nodes of Ranvier (Fig. 5C, ~15% increase), was several-fold greater than might have been expected from the calculated increase in OL density (~2%), estimated from the number of newly-formed EdU$^+$ CC1$^+$ OLs in good-performers at 1-day post-RAM (~50 new OLs per mm^2 per 25 μm section, Fig. 3D) relative to the total number of CC1+ OLs in the corpus callosum of P60-P90 mice (~3000 OLs per mm^2 per 25 μm section; Tripathi et al., 2017). This discrepancy could be explained by a combination of effects: 1) some (or many) OLs might be generated during RAM training by direct differentiation of OLPs without prior cell division (McKenzie et al.,2014; Xiao et al., 2016); such directly-generated OLs being invisible by EdU-labelling, 2) some very immature myelin-forming OLs might not yet express detectable levels of CC1 antigen, 3) the newly-formed internodes might be shorter on average than pre-existing internodes, as discussed above and 4) newly-formed OLs might make more internodes (hence

more nodes) than OLs generated earlier in life, as we showed previously for adult-born OLs in the mouse optic nerve (Young et al., 2013).

Discussion

Experimental blockade of OL genesis in adult *Myrf*-cKO mice has revealed that active production of new myelinating OLs supports motor skill learning and memory and the consolidation of remote (long-term) fear and spatial memories. We have now shown that active OL genesis is required for mice to improve their performance with training on T-maze and 8-arm radial maze tasks that exercise and assess spatial working memory – also known as delayed non-matching to position (DNMP) or win-shift behaviour (Rawlins and Olton, 1982; Sanderson and Bannerman 2011). *Myrf*-cKO mice did not improve their performance in these maze tasks over 8-9 days of post-habituation training – unlike their control littermates, which improved steadily during the training period. This demonstrates an inability of *Myrf*-cKO mice to improve their spatial working memory performance. The requirement for OL genesis in working memory training is intriguing because working memory capacity is known to underpin all kinds of cognitive abilities and correlates closely with measures of intelligence in humans and animals (Conway et al., 2003; Matzel and Kolata, 2010; Johnson et al., 2013; Takeuchi et al., 2018).

Remarkably, the performance of individual mice in our radial arm maze task correlated strongly with the numbers of additional OLPs and $CC1^+$ OLs generated by division and differentiation of OLPs during training. This suggests that OL generation and possibly myelination are directly and causally related to improved working memory performance. Enhanced OLP proliferation and differentiation into $CC1^+$ OLs were detected soon after training in both the gray matter of the prefrontal cortex and in the underlying sub-cortical white matter (genu). An increase in the number of myelin internodes, inferred from the presence of additional node/paranode structures, was also detected in the genu by EM. The ratio of node/paranode profiles to myelinated axon profiles was also increased post-training, consistent with the addition of shorter, nascent internodes. Over the subsequent 2 week post-training period the additional gray matter OLs disappeared, presumably through cell death and clearance, while a large proportion of those in white matter persisted longer-term. Thus, increased myelination of a subset of long-range axons in white matter might preserve the training-induced improvement in working memory for the mid- to long-term; it will be interesting in future to investigate the longer-term retention of these training effects and whether it correlates with the lifetime of the additional OLs and myelin.

Since EdU was provided to the mice during RAM training, the newly-formed EdU^+ $CC1^+$ OLs that we detected must have been generated from OLPs that divided during the training period. It is possible that a prior wave of new OLs was generated during training by direct differentiation of

OLPs without cell division, which could not have been detected by our present experiments. We previously found evidence for two waves of OL generation, before and after OLP division, during motor skills learning (McKenzie et al., 2014; Xiao et al., 2016). We speculated that direct OL differentiation temporarily depletes the OLP pool, which is then kicked into cell division by a homeostatic mechanism — e.g. through a temporary glut of mitogenic growth factors such as Pdgf (van Heyningen et al., 2001), or by loss of contact inhibition (Hughes et al., 2013) — in order to replenish the OLP population. Similar OL dynamics might occur during RAM training, in which case improvement of working memory might depend on direct OL differentiation, while OLP division and secondary OL differentiation consolidates the improvement. Alternatively, or in addition, enhanced OLP proliferation and the consequent increase in OLP population density, which persisted for at least 2 weeks post-training in the white matter, might itself lead to improved cognitive performance. There are reports that immature OL lineage cells in zebrafish (Marisca et al., 2020; Xiao et al., 2022) and mice (Buchanan et al., 2021; Auguste et al., 2022) can exert effects on neurons that are unrelated to myelination, including synaptic pruning by OLPs (Buchanan et al., 2021; Auguste et al., 2022). It is conceivable that such non-canonical effects could have a lasting impact on neural circuitry even if the responsible OL lineage cells are eventually eliminated.

The involvement of myelin in human cognition and particularly working memory has been suspected for some time (Nagy et al., 2004). For example, the spatial working memory performance of individual pre-adolescent children (ages 3-13) was found to correlate with fractional anisotropy (FA) in the superior longitudinal fasciculus, a white matter tract underlying the dorsal PFC, independent of chronological age (Vestergaard et al., 2011). FA is an MRI measure of the directional dependence of tissue diffusivity, believed to reflect, partly, the extent of myelination of aligned axons in white matter tracts. FA was also shown to increase (suggesting increased myelination) in task-relevant white matter tracts of young adults undertaking working memory training with the *N*-back test (Takeuchi et al., 2010). However, FA is at best an indirect measure of myelination; the histological and behavioural experiments we report here are the first unequivocal demonstration of a requirement for adaptive OL dynamics during working memory tasks in mice. Thus, improvements in working memory performance with training resembles motor skills training, in that both require reiterative practice over days and both rely on OL dynamics and presumably neo-myelination.

How might OL genesis and neo-myelination improve working memory performance? Neuronal activity persists (“reverberates”) within and among the pre-frontal cortex, parietal cortex and other brain areas (e.g. mediodorsal thalamus) for a limited period after the initial stimulus has ceased (the “delay” period). One long-held idea is that this reverberant activity maintains information in

working memory and that the power and decay time of the reverberations determine working memory capacity and duration (Goldman-Rakic, 1995; Wang et al., 2013; Bolkan et al., 2017; Leavitt, 2017; Rezayat et al., 2022). This general idea has been challenged by the discovery of activity-silent or latent working memory traces, held at the level of modified synapses (Mongillo et al., 2008; Rose et al., 2008; Wolff et al., 2015, 2017; Trubutschek et al., 2017). Despite this, it seems likely that both persistent neuronal activity and synaptic modification can co-contribute to working memory maintenance during the delay period (Constantinidis et al., 2018; Barbosa et al., 2020; Rezayat et al., 2022). If so, an expected outcome of working memory training might be to reinforce or prolong reverberatory activity, for which there is some evidence in humans (Olesen et al., 2004). It is conceivable that reverberation is limited by the energy required and available to maintain circuit activity, in which case myelination might improve working memory with reiterative training by 1) reducing the energy needed to propagate action potentials and 2) facilitating energy production within axons by providing them with metabolic substrates such as lactate (Saab et al., 2013).

Complex decision-making behaviours of several kinds, including those that rely on working memory, are associated with rhythmic electrical activity in multiple brain regions and particularly the coordination and coherence of rhythmicity among different regions (Buzsaki et al., 2012; Rezayat et al., 2022). Many studies have shown that increased coordination of rhythmic activities correlates with behavioural outcomes. For example, in an “H-maze” test of spatial working memory, phase synchrony between theta-rhythms (~4-12 Hz) in hippocampal CA1 and the medial prefrontal cortex (mPFC) increased when rats approached a choice-point of the maze prior to making a correct choice of goal-arm, but not prior to making an incorrect choice (Jones and Wilson, 2005). This long-range theta coherence resulted in coordinated firing of neurons in CA1 and mPFC, as a result of individual neurons firing at specific phases of the theta cycle in both regions (spike-phase locking). Theta-coherence between hippocampal and mPFC neurons was also observed in mice during the choice phase of a T-maze DNMP task (Sigurdsson et al., 2010). Moreover, theta-coherence increased during working memory training in the T-maze and, for individual mice, theta-coherence prior to training was predictive of subsequent learning ability (Sigurdsson et al., 2010). More recently, enhanced phase coupling between different frequency bands — between theta and beta (~12-30 Hz) or theta and gamma (~30-120 Hz) — has been linked to the accuracy of working memory-based decisions of mice in a T-maze DNMP task (Yamamoto et al., 2014; Tamura et al., 2017). Similar cross-frequency phase coupling correlates with working memory performance in primates, including humans (reviewed by Rezayat et al., 2022).

There is growing awareness that adaptive OL genesis and neo-myelination, by adjusting axonal conduction speeds, might play a key role in modulating and coordinating the sorts of rhythmic behaviours discussed above (Pajevic et al., 2014; Steadman et al., 2020; Noori et al., 2020). Simply put, faster communication between, say, hippocampus and PFC would be expected to allow hippocampal output to drive prefrontal circuits to oscillate more closely in tune with those in the hippocampus, or vice versa. It is not so obvious how adaptive myelination might drive the rapid changes in phase relationships that are observed during the execution of a behavioural task – as mice approach and pass a choice point in a maze, for example. However, this could be explained by positing that different components of a working memory task – a temporal sequence of events, for example – are represented by distinct non-overlapping assemblies of neurons in the PFC, that only one assembly is active at a given time and that the shifting oscillatory relationships between PFC and hippocampus result from rapid switching between the different assemblies (Luck and Vogel 2013). A recent live imaging study has demonstrated this organizational principle in macaques (Xie et al., 2022). It follows that the phase relationships between hippocampus and distinct PFC neuron assemblies could potentially be adjusted independently of one another, by adaptive myelination within the separate assemblies.

Working memory dysfunction and impaired inter-regional synchronicity are both features of common neurodegenerative disorders and psychiatric conditions including Alzheimer's and Parkinson's disease (Zokaei and Husain, 2019), schizophrenia (Sigurdsson et al., 2010), autism spectrum disorder (Bangel et al., 2014), attention deficit/ hyperactivity disorder (Jang et al., 2020) and others (reviewed by Uhlhaas and Singer 2006; Rezayat et al., 2022). There are also consistent reports of links between myelin dysregulation and schizophrenia (reviewed by Karoutzou et al., 2008; Takahashi et al., 2011). Hence, how adaptive myelination feeds into normal working memory and cognition, how disrupting those processes can lead to psychiatric disorders and how, in the longer term, this information might lead to benefits for affected individuals are important questions for the future.

Materials and Methods

Mice

Myrf$^{(flox/flox)}$: *Pdgfra-CreER*^{T2}*: Rosa26-YFP* mice were crossed to *Myrf*$^{(flox/+)}$: *Pdgfra-CreER*^{T2}*: Rosa26-YFP* on a mixed C57BL/6, CBA, 129 genetic background – mainly C57BL/6, although coat colour was agouti, hence CBA-derived. *Myrf* ^{flox} mice were originally from Ben Emery (Emery et al., 2009). *Pdgfra-CreER*^{T2} (Rivers et al., 2008) and *Rosa26-YFP* (Srinivas et al., 2001) were homozygous throughout. This cross generates similar numbers of *Myrf*$^{(flox/flox)}$*: Pdgfra-CreER*^{T2}*: Rosa26-YFP* (*Myrf*-cKO) and *Myrf*$^{(flox/+)}$*: Pdgfra-CreER*^{T2}: *Rosa26-YFP* (control) littermates that can

be distinguished by genotyping as previously described (McKenzie *et al*., 2014; Xiao *et al.,* 2016). *Pdgfra-CreER*^{T2} homozygosity was determined by qPCR using the following primers (5'-3'): TGACGGTGGGAGAATGTTAATC (Cre-f), GCTACACCAGAGACGGAAATC (Cre-r), ATGACA TCAAGAAGGTGGTG (GAPDH-f), CATACCAGGAAATGAGCTTG (GAPDH-r). Genotyping was carried out after behavioural testing so that the experimenter was blind to genotype during testing. The one exception was the left-right discrimination task, in which it was necessary to genotype prior to testing in order to be able to counterbalance numbers of *Myrf*-cKO and control mice between left and right goal-arms.

Tamoxifen and EdU

Tamoxifen (Sigma) was prepared on the day of administration by dissolving at a concentration of 40 mg/ml in corn oil by sonicating for one hour at 20-37ºC in a sonicating water bath. Tamoxifen was administered by oral gavage at a dose of 300 mg/kg once a day on four consecutive days (P60-P63). Mice were left to recover for 3 weeks before starting behavioural experiments. Experiments using mice were approved by the UCL Ethical Committee and authorized by the UK Home Office under the Animals (Scientific Procedures) Act 1986 and subsequent amendments.

To measure rates of cell generation, 5-ethynyl-2'-deoxyuridine (EdU) was administered via the drinking water at 0.2 mg/ml during T-maze or radial maze testing (8 or 9 days duration, respectively). For immunohistochemistry and EdU detection, mice were perfusion-fixed, then brains were removed under fixative and immersed overnight in 4% (w/v) paraformaldehyde in phosphate-buffered saline (PFA) on the final day of T-maze training, or either 1- or 14-days after the final day of radial arm maze training.

Mouse behaviour

Mice were maintained on an artificial 12 h light-dark cycle. Room lights were turned on at 7am and the dark period commenced at 7pm. Behavioural experiments were conducted between 9 am and 7 pm in a separate dedicated room. White noise at 75 dB was played throughout the day. Sessions were video-recorded for later analysis. For all experiments we used only behaviourally naïve male mice, which were group-housed at 2 to 5 mice per cage from weaning until the beginning of experiments.

T-maze rewarded alternation

The delayed non-matching to position (DNMP) task was carried out as described (Olton et al., 1978; Rawlins and Olton, 1982; Deacon and Rawlins, 2006) with modifications (Fig. 1 and Supplementary Video 1). At 11 weeks of age (P77), mice were caged singly and kept on a restricted diet of standard pellet chow to maintain them at a target ~85% of starting weight, to

motivate them to seek food rewards. Along with a measured amount of standard chow we provided the mice with 1 ml of dilute sweetened condensed milk (Carnation, Nestle; 50% (v/v) in distilled water) in their home cage for eight days up to and including the first day of habituation, to familiarize them with the food reward used during the task. During this time the mice were handled daily to gain familiarity with the experimenter.

After moving to the behaviour room, mice were left undisturbed in their home cages for 5 min prior to the start of any procedures in the maze. The T-maze consisted of a start-arm and two goal-arms, left and right, with a manually-operated door in each arm close to the T-junction. There were 3 days of habituation. On day 1, mice were released in the start-arm, facing away from the T-junction, with all doors removed (no food rewards present), and allowed to explore the maze freely for 30 min. This was the last day that condensed milk was provided in the home cage. On day 2, mice were introduced into the left or right goal-arm (with food rewards present), all doors closed, and allowed to consume the reward (70 μl dilute condensed milk) before being transferred to the opposite goal-arm and again allowed to consume the reward. This was repeated for all mice in the cohort and the whole sequence repeated five times, so that each mouse received 5 left-arm and 5 right-arm rewards on the day. This procedure was repeated on day 3 but starting in the opposite goal-arm. Each experimental trial consisted of a “forced” and a “free” run separated by a 30-second interval (delay) in the home cage. Both goal-arms were baited before starting the trial. In the forced run, either the left or right goal-arm was closed; the mouse was released in the start-arm and allowed to enter and consume the reward in the one accessible goal-arm. In the free run, both goal-arms were open and the mouse had to enter the previously closed/unvisited arm in order to receive a second reward. After a correct arm choice, the mouse was allowed to consume the reward before being removed to its home cage. After an incorrect arm choice the mouse was confined in the arm for 15 s before being removed to its home cage. Each mouse in the cohort completed its trial in turn and the whole cohort undertook 10 trials per day for the 8 days of the experiment with a between-trials interval for a given mouse of ~40 min. There were 5 left- and 5 right-arm forced runs per mouse per day, no more than 3 consecutive forced runs on the same side. The threshold time for one trial was 5 minutes and mice that exceeded this were removed from the analysis. The performance score on each day was calculated as the number of correct choices per 10 trials x 100 (%).

T-maze left-right discrimination

Experimentally naïve mice were assessed on their ability to acquire a simple left-right discrimination task using the same T-maze. This task places the same sensorimotor and motivational demands on mice but does not tax working memory. The apparatus and habituation steps were the same as for the rewarded alternation task. For each experimental trial, there was

only a single run and only one goal-arm was baited (70 μl dilute condensed milk). For a given mouse, the same arm was baited in all trials; for the different mice in the cohort left and right arms were counterbalanced. At the start of the trial the start-arm door was closed and both goal-arm doors open. The mouse was released in the start-arm, then the door was opened and the mouse was allowed to enter one of the arms in search of a food reward. After a correct arm choice, the mouse was allowed to consume the reward before being removed to its home cage. After an incorrect arm choice, the mouse was confined in the unrewarded arm for 15 s before being removed to its home cage. Each mouse in the cohort was tested in turn, then this whole sequence of trials repeated 10 times per day for 3 days with an inter-trial interval of ~40 min for each mouse, while other mice were in the maze. In the reversal phase of the task, the identity of the rewarded goal-arm was switched from left to right (or vice versa) for each mouse, and the whole experimental procedure repeated for another 3 days. The performance on each day was calculated as the number of correct choices per 10 trials x 100 (%).

8-arm radial maze

Spatial working memory was also assessed using a semi-automated 8-arm radial maze, purchased from Tracksys Ltd (Nottingham, UK). The RAM consists of a central octagonal hub with eight radiating arms 27 cm x 6 cm x 15 cm (length x width x height), entry to which is controlled by individual servo-driven doors that open/ close vertically from beneath the floor of the maze. The movement of mice in the maze was tracked by EthoVision XT13 video tracking and control software (Noldus, Wageningen, The Netherlands), programmed in-house (by T.S.) to operate the doors as required. The maze floor was illuminated evenly with indirect warm white light (about 80 lux at the centre) and white noise at ~75 dB was played during experiments. There were several distal visual cues such as a TV monitor and metallic ball above the maze and abstract symbols (Zener cards) on the ceiling above the maze. The distance travelled, mean speeds and acceleration were calculated by EthoVision XT13.

The RAM protocol was based on the protocol described for rats by Sasaki et al. (2018), modified for mice by T.S. with input from S.N. The procedure and feeding regimen in the week before habituation were the same as for the T-maze rewarded alternation task. There were 6 days of habituation on the RAM, divided into 3 stages of 2 days each. Days 1 and 2 were to allow the mice to explore the maze and to become accustomed to the movement and sound of the doors. Individual mice were placed in the central hub and doors to all arms (unbaited) were opened after 5 s initial confinement and mouse tracking started. After the mouse entered an arm the door to that arm was closed for 3 s (the duration of up/down door movement) before re-opening; then after leaving the arm the mouse was confined in the central hub for 3 s before all doors were re-opened. This sequence was repeated for 30 min. The mouse was then returned to its home cage and the

maze cleaned thoroughly. After day 2, condensed milk was no longer provided in the home cage. Days 3 and 4 introduced the mice to food rewards (70 μl of condensed milk diluted 1:1 with water), placed at the end of all arms in sunken wells so that they were not visible until the mice were within ~10 cm of the well. Mice were allowed to enter each arm at least twice without the doors operating to encourage free exploration (only the first visit was rewarded). Each mouse in the cohort undertook this habituation step twice daily with an ~40 min interval (while other mice were being run in the maze). Days 5 and 6 familiarized the mice to the combination of moving doors and food rewards; food rewards were present in all arms, the doors were operated as on days 1 and 2 and the trial was concluded after the mice had entered each arm at least once (only the first visit was rewarded). All mice in the cohort undertook two such sessions per day.

Habituation was followed by 9 days of RAM working memory training (Supplementary Videos 2-4). All arms were baited with diluted condensed milk (40 μl) at the start of each trial, which comprised 4 “forced runs” followed by a “free run”. In the forced runs, mice were initially confined to the central hub for 5 s, then admitted sequentially to 4 pseudo-randomly selected arms, no more than 3 of which were adjacent arms. Mice were confined to each arm for 15 s while consuming the reward, before opening the door to that and the subsequent arm simultaneously. Following their fourth and final forced run, they were confined to the central hub for 5 s before all doors opened together (and stayed open for the remainder of the task), allowing them to visit the 4 as-yet-unvisited arms and collect the remaining rewards. Once all rewards were collected, mice were allowed to enter 4 additional arms before being returned to their home cage, reinforcing the fact that rewards are not replenished. Each mouse completed 6 trials per day with a between-trials interval of ~45 min (while other mice were being tested). Working memory errors were recorded if mice entered an arm they had previously visited during either the forced or free runs. Trials were scored by “success rate” [4/ (4 + working memory errors)]. For example, if 4 arm visits were required to recover the 4 remaining rewards, the success rate was 4/4 or 100% (a “perfect trial”). If 8 arm visits were required, the success rate was 4/8 or 50%. Mice that scored ≥10 perfect trials over the 9 days of RAM training were defined as “good performers”, mice scoring ≤5 perfect trials were “poor performers”.

In the early stages of the test, mice tended to visit arms sequentially in either a clockwise or anticlockwise direction (daisy-chaining) (Supplementary Videos 2-4). We can calculate the average score that it is possible to attain by this strategy. For example, for the forced-arm pattern 1246 (numbered clockwise), daisy-chaining clockwise from arm 1 during the free run requires 8 arm visits to recover the remaining rewards (which are in arms 3578) (4 errors, 50% score); starting from arm 2 requires 7 visits (3 errors, 57% score); starting from arm 3 requires 6 visits (2 errors, 67% score) etc., average over all 8 start-arms ~55%. Performing the same calculation for

all the forced-run arm patterns that we employed gives an overall average score of ~55%. Control mice scored >75% after training, so they did not rely on daisy-chaining.

Novel object recognition task (NOR) and object location task (OLT)

Mice were allowed to explore an acrylic 30 cm x 30 cm x 40 cm white Perspex open field box for 10 min (habituation stage). External visual cues above the open field box included a wall-mounted book shelf, ceiling lights and CCD camera to record their performances. Two identical objects (non-toxic plaster models ~10 cm high) were then placed in the box in a symmetrical arrangement and the mice were allowed 5 min to investigate and become familiar with the objects. Either 10 min or 24 h later one of the objects was replaced with a novel object of similar size and material that the mice had never experienced before. At the same time the familiar object was replaced with an identical version that had been spray-cleaned with 70% ethanol and dried thoroughly at least 10 min previously. After object replacement the mice were allowed to investigate for another 5 min. The whole procedure including the exploratory stage was recorded using a video camera mounted on the ceiling. The time mice spent interacting with the objects – defined as physical contact with the object, or investigative activity in which the nose is pointing towards the object and no more than 2 cm from it – was assessed from the videos by two independent observers, blind to genotype. The NOR discrimination index is $(t_n – t_f)/ (t_n + t_f)$, where t_n is time spent interacting with the novel object and t_f is time interacting with the familiar object (Antunes and Biala, 2012), averaged between the two observers. A prior control experiment confirmed that mice did not spend more time interacting with one of the objects over the other when they were both introduced into the open field box at the same time.

The OLT was carried out as for NOR, with one modification. During the final test phase, instead of replacing one of the two identical objects with a novel object, one of them was moved to a new location in the box. The position of the displaced object was varied among mice. The OLT discrimination index is $(t_n – t_f)/ (t_n + t_f)$, where t_n is time spent interacting with the object in the new location and t_f is time interacting with the object in the familiar location.

Open field test (OFT)

The initial habituation stage of the NOR and OLT tasks, in the absence of any objects, doubled as an open-field test. Ten each of the NOR and OLT trials were selected randomly for analysis, prior to the tests having been conducted. ActualTrack software (Actual Analytics Ltd, Edinburgh, UK) was used to track mouse movements in during the 10 min test. The mean speeds and distances travelled by mice were calculated by the software, along with heat maps and bird nest maps of their trajectories.

Histology and cell counts

Following behavioural tests, mice were transcardially perfused with 4% (w/v) paraformaldehyde (PFA, Sigma) in phosphate-buffered saline (PBS). Brains were dissected and post-fixed by immersion in 4% PFA overnight at 4ºC. The following day, brain tissue was cryoprotected in 20% (w/v) sucrose in diethyl pyrocarbonate (DEPC)-treated PBS until the tissue sank, before embedding in OCT compound (Tissue-Tek) for cryo-sectioning. Coronal brain cryosections (25 µm) were collected and stored in 0.02% (w/v) sodium azide in PBS at 4ºC until needed. Immunostaining was as previously described (McKenzie et al., 2014, Xiao et al., 2016). To permeabilize the tissue and block non-specific binding, sections were treated with blocking solution [10% (v/v) fetal bovine serum, 0.5% (v/v) Triton X-100 in PBS] for 2 h at 20-25ºC. Primary and secondary antibodies were diluted in 0.1% (v/v) Triton X-100 and 5% FBS in PBS. Primary antibody incubation was overnight at 4ºC. Secondary antibodies (Invitrogen, 1:1,000 dilution) were applied together with Hoechst 33258 DNA dye (Sigma-Aldrich, 0.2 µg/ml) for 2 h at 20-25ºC. Primary antibodies were anti-Olig2 (rabbit, Merck AB9610, 1:500), monoclonal CC1 (mouse, Calbiochem OP80, 1:200), anti-YFP (chicken, Aves labs, 1:1,000), anti-Pdgfra (rabbit, Cell Signalling Technology 3164S, 1:200), anti-Caspr clone K65/35 (mouse, Merck MABN69, 1:300), anti-$Na_V1.6$ (rabbit, Alomone ASC-009,1:500). EdU detection using the Alexa Fluor 555 Click-iT kit (Invitrogen) was performed prior to blocking, according the manufacturer's instructions. For node analysis, primary antibodies were incubated for 3 days at 4ºC, and secondary antibodies were applied overnight at 4ºC (Arancibia-Carcamo et al., 2017).

Confocal images were taken using a Zeiss 880 Airyscan at 0.8-1.2 µm spacing in the Z-dimension. Cells were counted in tiled coronal images (20 µm Z-stacks) from the corpus callosum (Bregma +1.0 mm), anterior cingulate cortex (Bregma +1.0 mm), prelimbic and infralimbic cortex (Bregma +1.4 mm), hippocampus and fimbria (Bregma –1.8 mm) — two to four sections from each region per brain, from three or more brains of each experimental group. Images were taken by S.G.N., re-labelled by M.G. before counting by S.G.N., blind to genotype, then decoded by M.G. Prism 9.0 (GraphPad) was used for statistical analysis. Nodes of Ranvier were counted in 5 µm thick Z-stacks in coronal sections of corpus callosum (Bregma +1.0 mm).

Node and paranode length measurements

Node and paranode lengths were analyzed as described by Arancibia-Cárcamo et al. (2017). Briefly, confocal images of the anterior corpus callosum (Bregma +1.0 mm) were taken at 0.38 µm optical slice intervals. Using ImageJ, images were background subtracted and maximum intensity projections were generated using a maximum stack thickness of 2.32 µm. A line intensity profile was drawn in IMAGEJ, spanning both Caspr-immunolabelled paranodes flanking nodal $Na_V1.6$ immunolabelling. The length of the node was then calculated using a MATLAB (The MathWorks

Inc.) script (kindly provided by Tania Quintela-López and David Attwell, UCL) that estimates the distance between the half-maximum intensities of Caspr immunofluorescence at each end of the node. To assess paranodal length, the script was modified to estimate the distance between the half-maximum Caspr immunofluorescence intensities at either end of the paranode. Total length of the node/paranode structure was the sum of the lengths of the node and both paranodes.

Electron microscopy

One day after RAM training, mice were perfusion-fixed with 2.5% (v/v) glutaraldehyde and 2% (w/v) PFA in 0.1 M sodium cacodylate buffer (pH 7.4). Brains were post-fixed by immersion in the same fixative overnight at 4ºC, before transferring to 0.1 M PBS for shipment from UK at ambient temperature. In Japan, thick sagittal slices were prepared at <1 mm thickness from 4.5 x 2 mm tissue blocks containing the whole length of the corpus callosum. The sections were immersed in 1% (w/v) osmium tetroxide solution for 2 h at 4ºC, dehydrated through a series of graded alcohols and embedded in Epon 812 resin (TAAB Laboratories, UK). Ultrathin parasagittal sections (100 nm) were cut on an ultramicrotome (Ultracut UCT, Leica) and collected on tin-coated glass slides, stained with uranyl acetate and lead citrate and imaged in a scanning EM equipped with a back-scattered electron beam detector (Hitachi SU8010) at 1.0 – 1.5 kV accelerating voltage, for quantifying axon-myelin units and nodes of Ranvier. Cross-sectional profiles of myelinated axons, paranodes and nodes (Fig. 5) were counted in Japan by K.T., blind to genotype; brain samples were codified prior to shipping and the data subsequently decoded in the U.K.

Statistics

Statistical significance was determined using GraphPad Prism (GraphPad Software, CA, USA) and OriginPro software. Normality of data distribution was assessed using Kolmogorov–Smirnov and Shapiro-Wilk tests. Data are presented as median ± interquartile range (25% and 75%). Repeated measures two-way Analysis of Variance (ANOVA) was used to compare behavioural performance across groups over time in the T-maze and RAM tasks (Fig. 1). Unpaired Student's t-tests were used for other behavioural experiments (Supplementary Fig, S1) unless otherwise specified. P-values were corrected for multiple comparisons using Šídák or Tukey post-tests as specified. The cell counts of Fig. 3 and Fig. S3 were compared using the Kruskal-Wallis non-parametric test; p-values were corrected for multiple comparisons using the Benjamini-Krieger-Yekutieli false discovery rate test (Benjamini et al., 2006). A simple linear regression model using a least squares regression without weighting was applied to good and poor performers in Fig. 4 to generate a line of best fit with 95% confidence bands. The goodness-of-fit of the line is represented by the coefficient of determination R^2. Algebraic equations for the lines of best fit together with their R^2 values are given in Supplementary Table 3. Each line of best fit was subjected to an extra sum-of-squares F-test against a theoretical gradient of zero to determine

whether the gradient of the line was significantly different from zero, demonstrating positive correlation.

Counts of internode/node/paranode profiles (Fig. 5) in good performers versus home cage controls were compared using Student's two-tailed t-test. p-values are indicated in the figures: n.s. (not significant, $p > 0.05$), * ($p \leq 0.05$), ** ($p \leq 0.01$), *** ($p \leq 0.001$), **** ($p \leq 0.0001$).

Display items

Illustrations for figures were created using BioRender.com. Graphs were generated in GraphPad and annotated and arranged using Adobe Photoshop.

Acknowledgements

We thank our colleagues at UCL for help, advice and discussion. We especially thank Tomohito Hanasaka and all members of the Technical Support Center for Life Science Research at Iwate Medical University for providing expertise in electron microscopy and morphometric analysis. We also thank Tania Quintela-López and David Attwell (UCL) for advice about node/paranode immunolabelling and analysis and for providing us with their MATLAB script. This work was supported by the Wellcome Trust (108726/Z/15/Z and 214286/Z/18/Z to W.D.R.). H.J.-B. and the Wellcome Centre for Integrative Neuroimaging were supported by the Wellcome Trust (222446/Z/21/Z and 203139/Z/16/Z).

Author contributions

T.S. and W.D.R. conceived the project. W.D.R. obtained funding. T.S., S.N., M.S., K.T. and W.D.R. designed the experiments with input from H.J.-B. and D.B. The experiments were performed by T.S, S.N., M.S., Y.J., K.O, and K.T. with technical assistance from M.G. K.O. provided EM facilities and expertise. S.N., T.S., K.T. and W.D.R. interpreted the data and wrote the paper with input from the other authors.

References

Antunes, M., and Biala, G. (2012). The novel object recognition memory: neurobiology, test procedure, and its modifications. *Cogn Process* **13**, 93-110.

Arancibia-Carcamo, I.L., Ford, M.C., Cossell, L., Ishida, K., Tohyama, K., and Attwell, D. (2017). Node of Ranvier length as a potential regulator of myelinated axon conduction speed. *eLife* **6**. doi:10.7554/eLife.23329

Auguste, Y.S.S., Ferro, A., Kahng, J.A., Xavier, A.M., Dixon, J.R., Vrudhula, U., Nichitiu, A.S., Rosado, D., Wee, T.L., Pedmale, U.V.*, et al.* (2022). Oligodendrocyte precursor cells engulf

synapses during circuit remodeling in mice. *Nat Neurosci* **25**, 1273-1278. (Publisher Correction: *Nat Neurosci* **25**, 1735.)

Bacmeister, C.M., Barr, H.J., McClain, C.R., Thornton, M.A., Nettles, D., Welle, C.G., and Hughes, E.G. (2020). Motor learning promotes remyelination via new and surviving oligodendrocytes. *Nat Neurosci* **23**, 819-831.

Bacmeister, C.M., Huang, R., Osso, L.A., Thornton, M.A., Conant, L., Chavez, A.R., Poleg-Polsky, A., and Hughes, E.G. (2022). Motor learning drives dynamic patterns of intermittent myelination on learning-activated axons. *Nat Neurosci* **25**, 1300-1313.

Baddeley, A. (2010). Working memory. *Curr Biol* **20**, R136-140.

Bangel, K.A., Batty, M., Ye, A.X., Meaux, E., Taylor, M.J., and Doesburg, S.M. (2014). Reduced beta band connectivity during number estimation in autism. *Neuroimage Clin* **6**, 202-213.

Bannerman, D.M., Sprengel, R., Sanderson, D.J., McHugh, S.B., Rawlins, J.N., Monyer, H., and Seeburg, P.H. (2014). Hippocampal synaptic plasticity, spatial memory and anxiety. *Nature reviews Neuroscience* **15**, 181-192.

Barbosa, J., Stein, H., Martinez, R.L., Galan-Gadea, A., Li, S., Dalmau, J., Adam, K.C.S., Valls-Sole, J., Constantinidis, C., and Compte, A. (2020). Interplay between persistent activity and activity-silent dynamics in the prefrontal cortex underlies serial biases in working memory. *Nat Neurosci* **23**, 1016-1024.

Benjamini, Y., Krieger, A.M., Yekutieli, D. (2006). Adaptive linear step-up procedures that control the false discovery rate. *Biometrika* **93**, 491-507.

Bergles, D.E., and Richardson, W.D. (2015). Oligodendrocyte development and plasticity. *Cold Spring Harb Perspect Biol* **8**, a020453. doi:10.1101/cshperspect.a020453

Bergles, D.E., Roberts, J.D., Somogyi, P., and Jahr, C.E. (2000). Glutamatergic synapses on oligodendrocyte precursor cells in the hippocampus. *Nature* **405**, 187-191.

Bolkan, S.S., Stujenske, J.M., Parnaudeau, S., Spellman, T.J., Rauffenbart, C., Abbas, A.I., Harris, A.Z., Gordon, J.A., and Kellendonk, C. (2017). Thalamic projections sustain prefrontal activity during working memory maintenance. *Nat Neurosci* **20**, 987-996.

Buchanan, J.E.A. (2021). Oligodendrocyte progenitor cells prune axons in the mouse neocortex. *BioRxiv*. doi:10.1101/2021.05.29.446047

Buzsaki, G., Anastassiou, C.A., and Koch, C. (2012). The origin of extracellular fields and currents--EEG, ECoG, LFP and spikes. *Nature reviews Neuroscience* **13**, 407-420.

Chai, W.J., Abd Hamid, A.I., and Abdullah, J.M. (2018). Working memory from the psychological and neurosciences perspectives: a review. *Front Psychol* **9**, 401. doi:10.3389/fpsyg.2018.00401

Constantinidis, C., Funahashi, S., Lee, D., Murray, J.D., Qi, X.L., Wang, M., and Arnsten, A.F.T. (2018). Persistent spiking activity underlies working memory. *J Neurosci* **38**, 7020-7028.

Conway, A.R., Kane, M.J., and Engle, R.W. (2003). Working memory capacity and its relation to general intelligence. *Trends Cogn Sci* **7**, 547-552.

Cowan, N. (2008). What are the differences between long-term, short-term, and working memory? *Prog Brain Res* **169**, 323-338.

D'Esposito, M., and Postle, B.R. (2015). The cognitive neuroscience of working memory. *Annu Rev Psychol* **66**, 115-142.

Dahmani, L., Courcot, B., Near, J., Patel, R., Amaral, R.S.C., Chakravarty, M.M., and Bohbot, V.D. (2019). Fimbria-fornix volume is associated with spatial memory and olfactory identification in humans. *Front Syst Neurosci* **13**, 87. doi:10.3389/fnsys.2019.00087

Deacon, R.M., and Rawlins, J.N. (2006). T-maze alternation in the rodent. *Nat Protoc* **1**, 7-12.

Emery, B., Agalliu, D., Cahoy, J.D., Watkins, T.A., Dugas, J.C., Mulinyawe, S.B., Ibrahim, A., Ligon, K.L., Rowitch, D.H., and Barres, B.A. (2009). Myelin gene regulatory factor is a critical transcriptional regulator required for CNS myelination. *Cell* **138**, 172-185.

Etxeberria, A., Hokanson, K.C., Dao, D.Q., Mayoral, S.R., Mei, F., Redmond, S.A., Ullian, E.M., and Chan, J.R. (2016). Dynamic modulation of myelination in response to visual stimuli alters optic nerve conduction velocity. *J Neurosci* **36**, 6937-6948.

Gibson, E.M., Purger, D., Mount, C.W., Goldstein, A.K., Lin, G.L., Wood, L.S., Inema, I., Miller, S.E., Bieri, G., Zuchero, J.B., et al. (2014). Neuronal activity promotes oligodendrogenesis and adaptive myelination in the mammalian brain. *Science* **344**, 1252304. doi:10.1126/science.1252304

Goldman-Rakic, P.S. (1995). Cellular basis of working memory. *Neuron* **14**, 477-485.

Guye, S., and von Bastian, C.C. (2017). Working memory training in older adults: Bayesian evidence supporting the absence of transfer. *Psychol Aging* **32**, 732-746.

Hughes, E.G., Kang, S.H., Fukaya, M., and Bergles, D.E. (2013). Oligodendrocyte progenitors balance growth with self-repulsion to achieve homeostasis in the adult brain. *Nat Neurosci* **16**, 668-676.

Hughes, E.G., Orthmann-Murphy, J.L., Langseth, A.J., and Bergles, D.E. (2018). Myelin remodeling through experience-dependent oligodendrogenesis in the adult somatosensory cortex. *Nat Neurosci* **21**, 696-706.

Jang, K.M., Kim, M.S., and Kim, D.W. (2020). The dynamic properties of a brain network during spatial working memory tasks in college students with ADHD traits. *Front Hum Neurosci* **14**, 580813. doi:10.3389/fnhum.2020.580813

Johnson, M.K., McMahon, R.P., Robinson, B.M., Harvey, A.N., Hahn, B., Leonard, C.J., Luck, S.J., and Gold, J.M. (2013). The relationship between working memory capacity and broad measures of cognitive ability in healthy adults and people with schizophrenia. *Neuropsychology* **27**, 220-229.

Jones, M.W., and Wilson, M.A. (2005). Theta rhythms coordinate hippocampal-prefrontal interactions in a spatial memory task. *PLoS Biol* **3**, e402. doi:10.1371/journal.pbio.0030402

Karoutzou, G., Emrich, H.M., and Dietrich, D.E. (2008). The myelin-pathogenesis puzzle in schizophrenia: a literature review. *Mol Psychiatry **13***, 245-260.

Kougioumtzidou, E., Shimizu, T., Hamilton, N.B., Tohyama, K., Sprengel, R., Monyer, H., Attwell, D., and Richardson, W.D. (2017). Signalling through AMPA receptors on oligodendrocyte precursors promotes myelination by enhancing oligodendrocyte survival. *eLife* **6**. doi:10.7554/eLife.28080

Leavitt, M.L., Mendoza-Halliday, D., and Martinez-Trujillo, J.C. (2017). Sustained activity encoding working memories: not fully distributed. *Trends Neurosci* **40**, 328-346.

Light, K.R., Kolata, S., Wass, C., Denman-Brice, A., Zagalsky, R., and Matzel, L.D. (2010). Working memory training promotes general cognitive abilities in genetically heterogeneous mice. *Curr Biol* **20**, 777-782.

Linares, R., Borella, E., Lechuga, M.T., Carretti, B., and Pelegrina, S. (2018). Training working memory updating in young adults. *Psychol Res* **82**, 535-548.

Luck, S.J., and Vogel, E.K. (2013). Visual working memory capacity: from psychophysics and neurobiology to individual differences. *Trends Cogn Sci* **17**, 391-400.

Marisca, R., Hoche, T., Agirre, E., Hoodless, L.J., Barkey, W., Auer, F., Castelo-Branco, G., and Czopka, T. (2020). Functionally distinct subgroups of oligodendrocyte precursor cells integrate neural activity and execute myelin formation. *Nat Neurosci* **23**, 363-374.

Matzel, L.D., and Kolata, S. (2010). Selective attention, working memory, and animal intelligence. *Neurosci Biobehav Rev* **34**, 23-30.

McHugh, S.B., and Bannerman, D.M. (2010). Cognition: learning and memory: spatial. In *Encyclopedia of Behavioral Neuroscience*, G. Koob, Le Moal, M., Thompson, R., eds. (Elsevier Science), pp. 279-287.

McKenzie, I.A., Ohayon, D., Li, H., de Faria, J.P., Emery, B., Tohyama, K., and Richardson, W.D. (2014). Motor skill learning requires active central myelination. *Science* **346**, 318-322.

Milner, B., Squire, L.R., and Kandel, E.R. (1998). Cognitive neuroscience and the study of memory. *Neuron* **20**, 445-468.

Mitew, S., Gobius, I., Fenlon, L.R., McDougall, S.J., Hawkes, D., Xing, Y.L., Bujalka, H., Gundlach, A.L., Richards, L.J., Kilpatrick, T.J.*, et al.* (2018). Pharmacogenetic stimulation of neuronal activity increases myelination in an axon-specific manner. *Nat Commun* **9**, 306. doi:10.1038/s41467-017-02719-2

Mongillo, G., Barak, O., and Tsodyks, M. (2008). Synaptic theory of working memory . *Science* **319**, 1543-1546.

Nagy, Z., Westerberg, H., and Klingberg, T. (2004). Maturation of white matter is associated with the development of cognitive functions during childhood. *J Cogn Neurosci* **16**, 1227-1233.

Noori, R., Park, D., Griffiths, J.D., Bells, S., Frankland, P.W., Mabbott, D., and Lefebvre, J. (2020). Activity-dependent myelination: A glial mechanism of oscillatory self-organization in large-scale brain networks. *Proc Natl Acad Sci USA* **117**, 13227-13237.

Olesen, P.J., Westerberg, H., and Klingberg, T. (2004). Increased prefrontal and parietal activity after training of working memory. *Nat Neurosci* **7**, 75-79.

Olton, D. S., Walker, J.A., and Gage, F.H. (1978). Hippocampal connections and spatial discrimination. Brain Res **139**, 295-308.

Olton, D.S., and Papas, B.C. (1979). Spatial memory and hippocampal function. *Neuropsychologia* **17**, 669-682.

Pajevic, S., Basser, P.J., and Fields, R.D. (2014). Role of myelin plasticity in oscillations and synchrony of neuronal activity. *Neuroscience* **276**, 135-147.

Pan, S., Mayoral, S.R., Choi, H.S., Chan, J.R., and Kheirbek, M.A. (2020). Preservation of a remote fear memory requires new myelin formation. *Nat Neurosci* **23**, 487-499.

Rawlins, J.N., and Olton, D.S. (1982). The septo-hippocampal system and cognitive mapping. *Behav Brain Res* **5**, 331-358.

Rezayat, E., Clark, K., Dehaqani, M.A., and Noudoost, B. (2021). Dependence of working memory on coordinated activity across brain areas. *Front Syst Neurosci* **15**, 787316. doi:10.3389/fnsys.2021.787316

Rivers, L.E., Young, K.M., Rizzi, M., Jamen, F., Psachoulia, K., Wade, A., Kessaris, N., and Richardson, W.D. (2008). PDGFRA/NG2 glia generate myelinating oligodendrocytes and piriform projection neurons in adult mice. *Nat Neurosci* **11**, 1392-1401.

Rose, N.S., LaRocque, J.J., Riggall, A.C., Gosseries, O., Starrett, M.J., Meyering, E.E., and Postle, B.R. (2016). Reactivation of latent working memories with transcranial magnetic stimulation. *Science* **354**, 1136-1139.

Saab, A.S., Tzvetanova, I.D., and Nave, K.A. (2013). The role of myelin and oligodendrocytes in axonal energy metabolism. *Curr Opin Neurobiol* **23**, 1065-1072.

Sampaio-Baptista, C., Khrapitchev, A.A., Foxley, S., Schlagheck, T., Scholz, J., Jbabdi, S., DeLuca, G.C., Miller, K.L., Taylor, A., Thomas, N.*, et al.* (2013). Motor skill learning induces changes in white matter microstructure and myelination. *J Neurosci* **33**, 19499-19503.

Sanderson, D.J., and Bannerman, D.M. (2011). Competitive short-term and long-term memory processes in spatial habituation. *J Exp Psychol Anim Behav Process* **37**, 189-199.

Sasaki, T., Piatti, V.C., Hwaun, E., Ahmadi, S., Lisman, J.E., Leutgeb, S., and Leutgeb, J.K. (2018). Dentate network activity is necessary for spatial working memory by supporting CA3 sharp-wave ripple generation and prospective firing of CA3 neurons. *Nat Neurosci* **21**, 258-269.

Scholz, J., Klein, M.C., Behrens, T.E., and Johansen-Berg, H. (2009). Training induces changes in white-matter architecture. *Nat Neurosci* **12**, 1370-1371.

Sigurdsson, T., Stark, K.L., Karayiorgou, M., Gogos, J.A., and Gordon, J.A. (2010). Impaired hippocampal-prefrontal synchrony in a genetic mouse model of schizophrenia. *Nature* **464**, 763-767.

Spellman, T., Rigotti, M., Ahmari, S.E., Fusi, S., Gogos, J.A., and Gordon, J.A. (2015). Hippocampal-prefrontal input supports spatial encoding in working memory. *Nature* **522**, 309-314.

Srinivas, S., Watanabe, T., Lin, C.S., William, C.M., Tanabe, Y., Jessell, T.M., and Costantini, F. (2001). Cre reporter strains produced by targeted insertion of EYFP and ECFP into the ROSA26 locus. *BMC Dev Biol* **1**, 4. doi:10.1186/1471-213x-1-4

Steadman, P.E., Xia, F., Ahmed, M., Mocle, A.J., Penning, A.R.A., Geraghty, A.C., Steenland, H.W., Monje, M., Josselyn, S.A., and Frankland, P.W. (2020). Disruption of oligodendrogenesis impairs memory consolidation in adult mice. *Neuron* **105**, 150-164 e156. doi:10.1016/j.neuron.2019.10.013

Swire, M., Kotelevtsev, Y., Webb, D.J., Lyons, D.A., and Ffrench-Constant, C. (2019). Endothelin signalling mediates experience-dependent myelination in the CNS. *eLife* **8**. doi:10.7554/eLife.49493

Takahashi, N., Sakurai, T., Davis, K.L., and Buxbaum, J.D. (2011). Linking oligodendrocyte and myelin dysfunction to neurocircuitry abnormalities in schizophrenia. *Prog Neurobiol* **93**, 13-24.

Takeuchi, H., Sekiguchi, A., Taki, Y., Yokoyama, S., Yomogida, Y., Komuro, N., Yamanouchi, T., Suzuki, S., and Kawashima, R. (2010). Training of working memory impacts structural connectivity. *J Neurosci* **30**, 3297-3303.

Takeuchi, H., Taki, Y., Nouchi, R., Yokoyama, R., Kotozaki, Y., Nakagawa, S., Sekiguchi, A., Iizuka, K., Hanawa, S., Araki, T.*, et al.* (2018). General intelligence is associated with working memory-related brain activity: new evidence from a large sample study. *Brain Struct Funct* **223**, 4243-4258.

Tamura, M., Spellman, T.J., Rosen, A.M., Gogos, J.A., and Gordon, J.A. (2017). Hippocampal-prefrontal theta-gamma coupling during performance of a spatial working memory task. *Nat Commun* **8**, 2182. doi:10.1038/s41467-017-02108-9

Tripathi, R.B., Jackiewicz, M., McKenzie, I.A., Kougioumtzidou, E., Grist, M., and Richardson, W.D. (2017). Remarkable stability of myelinating oligodendrocytes in mice. *Cell Rep* **21**, 316-323.

Trubutschek, D., Marti, S., Ojeda, A., King, J.R., Mi, Y., Tsodyks, M., and Dehaene, S. (2017). A theory of working memory without consciousness or sustained activity. *eLife* **6**. doi:10.7554/eLife.23871

Uhlhaas, P.J., and Singer, W. (2006). Neural synchrony in brain disorders: relevance for cognitive dysfunctions and pathophysiology. *Neuron* **52**, 155-168.

van Heyningen, P., Calver, A.R., and Richardson, W.D. (2001). Control of progenitor cell number by mitogen supply and demand. *Curr Biol* **11**, 232-241.

Vestergaard, M., Madsen, K.S., Baare, W.F., Skimminge, A., Ejersbo, L.R., Ramsoy, T.Z., Gerlach, C., Akeson, P., Paulson, O.B., and Jernigan, T.L. (2011). White matter microstructure in superior longitudinal fasciculus associated with spatial working memory performance in children. *J Cogn Neurosci* **23**, 2135-2146.

Wang, M., Yang, Y., Wang, C.J., Gamo, N.J., Jin, L.E., Mazer, J.A., Morrison, J.H., Wang, X.J., and Arnsten, A.F. (2013). NMDA receptors subserve persistent neuronal firing during working memory in dorsolateral prefrontal cortex. *Neuron* **77**, 736-749.

Wolff, M.J., Ding, J., Myers, N.E., and Stokes, M.G. (2015). Revealing hidden states in visual working memory using electroencephalography. *Front Syst Neurosci* **9**, 123. doi:10.3389/fnsys.2015.00123

Wolff, M.J., Jochim, J., Akyurek, E.G., and Stokes, M.G. (2017). Dynamic hidden states underlying working-memory-guided behavior. *Nat Neurosci* **20**, 864-871.

Xiao, L., Ohayon, D., McKenzie, I.A., Sinclair-Wilson, A., Wright, J.L., Fudge, A.D., Emery, B., Li, H., and Richardson, W.D. (2016). Rapid production of new oligodendrocytes is required in the earliest stages of motor-skill learning. *Nat Neurosci* **19**, 1210-1217.

Xiao, Y., Petrucco, L., Hoodless, L.J., Portugues, R., and Czopka, T. (2022). Oligodendrocyte precursor cells sculpt the visual system by regulating axonal remodeling. *Nat Neurosci* **25**, 280-284.

Xie, Y., Hu, P., Li, J., Chen, J., Song, W., Wang, X.J., Yang, T., Dehaene, S., Tang, S., Min, B.*, et al.* (2022). Geometry of sequence working memory in macaque prefrontal cortex. *Science* **375**, 632-639.

Yamamoto, J., Suh, J., Takeuchi, D., and Tonegawa, S. (2014). Successful execution of working memory linked to synchronized high-frequency gamma oscillations. *Cell* **157**, 845-857.

Young, K.M., Psachoulia, K., Tripathi, R.B., Dunn, S.J., Cossell, L., Attwell, D., Tohyama, K., and Richardson, W.D. (2013). Oligodendrocyte dynamics in the healthy adult CNS: evidence for myelin remodeling. *Neuron* **77**, 873-885.

Zokaei, N., and Husain, M. (2019). Working memory in Alzheimer's disease and Parkinson's disease. *Curr Top Behav Neurosci*, 325-344.

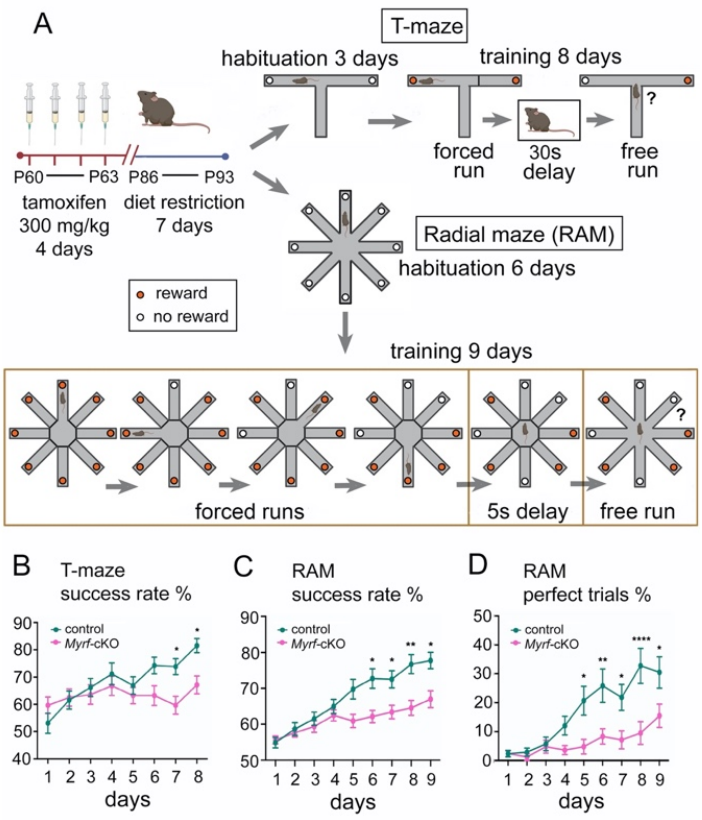

Figure 1. Working memory training requires OL generation.

(**A**) T-maze and radial arm maze (RAM) protocols. (**B**) Success rates of control (n=26) and *Myrf*-cKO (n=28) adult male mice during T-maze training. Controls improved their success rate over the 8 days of training whereas *Myrf*-cKOs barely improved [repeated measures 2-way ANOVA: time x genotype p=0.0012, F(7, 364) = 3.50; time, p<0.0001, F(7, 364) = 7.16; genotype, p=0.066, F(1, 52) = 3.52]. Controls attained a significantly greater success rate on the final two days of T-maze training compared to *Myrf*-cKOs (Day 7: control 74% ± 2.9%, *Myrf*-cKO 60% ± 3.3%, p=0.02. Day 8: control 82% ± 2.6%, *Myrf*-cKO 67% ± 3.3%, p=0.009, Šídák's post-test). (**C**) Success rates of control (n=28) and *Myrf*-cKO (n=29) adult male mice over 9 days of RAM training [repeated measures 2-way ANOVA: time x genotype p<0.0001, F(8, 440) = 7.41; time p<0.0001, F(4, 239) = 39.8; genotype p=0.009, F(1, 55) = 7.5]. Controls surpassed *Myrf*-cKOs on days 6-9 (e.g. Day 8: control 77% ± 3%, *Myrf*-cKO 65% ± 2% p=0.006. Day 9: control 78% ± 2%, *Myrf*-cKO 67% ± 2%, p=0.02. Šídák's post-test). (**D**) Fraction (%) of trials over the full 9 days of RAM testing in which mice recorded no working memory errors ("perfect trials") [repeated measures 2-way ANOVA: time x genotype p<0.0001, F(8, 440) = 5.4; time p<0.0001, F(8, 440) = 19; genotype p=0.006, F(1, 55) = 8.1]. Control mice recorded more perfect trials than *Myrf*-cKOs on days 5-9 (e.g. Day 8: control 33% ± 6%, *Myrf*-cKO 10% ± 4%, p<0.0001. Day 9: control 31% ± 5%, *Myrf*-cKO 16% ± 4%, p=0.03. Šídák's post-test).

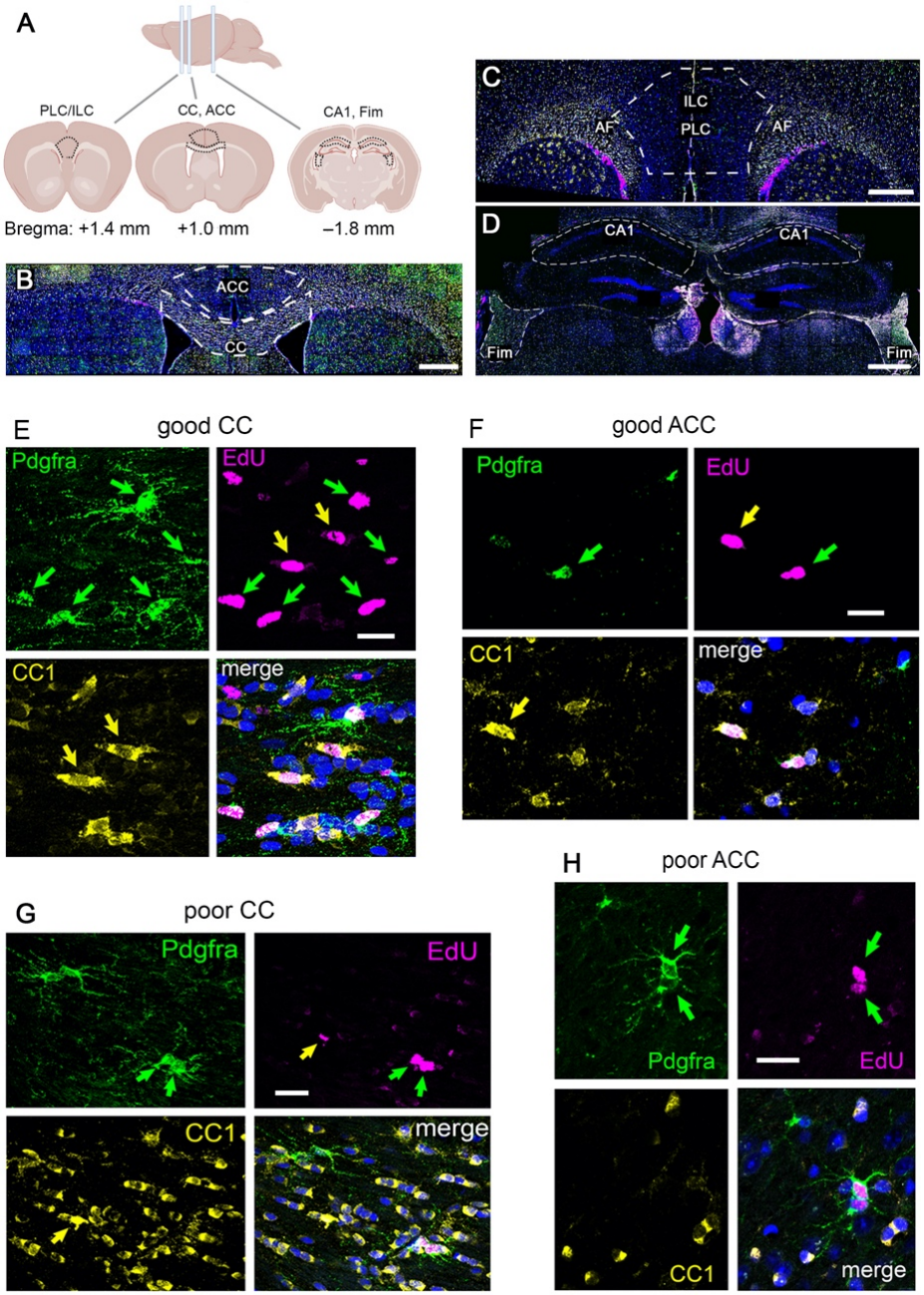

Figure 2. **Immunofluorescence analysis of OL lineage cells.** (**A**) Coronal sections through the brains of RAM-trained mice (1- or 14-days post-training) or home cage controls were analyzed at the level of the anterior cingulate cortex (ACC) (~Bregma +1.4 mm), prelimbic/ infralimbic cortex (PLC/ILC) (~Bregma 1.0 mm), hippocampus (CA1) and Fimbria (Fim) (~Bregma –1.8 mm). OL lineage cells were identified by immunolabelling with anti-Pdgfra (for OLPs) and monoclonal CC1 (for differentiated OLs), together with EdU histochemistry to identify recently-divided cells and their progeny. Sections were post-stained with Hoechst dye (blue) to label cell nuclei. (**B**-**D**) Low-magnification images illustrating the areas analyzed: (**B**) ACC and underlying anterior corpus callosum (CC), (**C**) PLC/ILC, (**D**) hippocampal CA1 and Fimbria. (**E-H**) Representative higher-

magnification images of OL lineage cells in the ACC and CC of mice that we categorized as either good- (**E**, **F**) or poor-performers (**G**, **H**) in the RAM task (≥10 or ≤5 "perfect trials" during the 9 days of RAM training/testing). *Green arrows*, recently-divided EdU^+ $Pdgfra^+$ OLPs; *yellow arrows* newly-formed EdU^+ $CC1^+$ OLs. *Scale bars:* (**B**-**D**), 1 mm; (**E**-**H**), 20 μm.

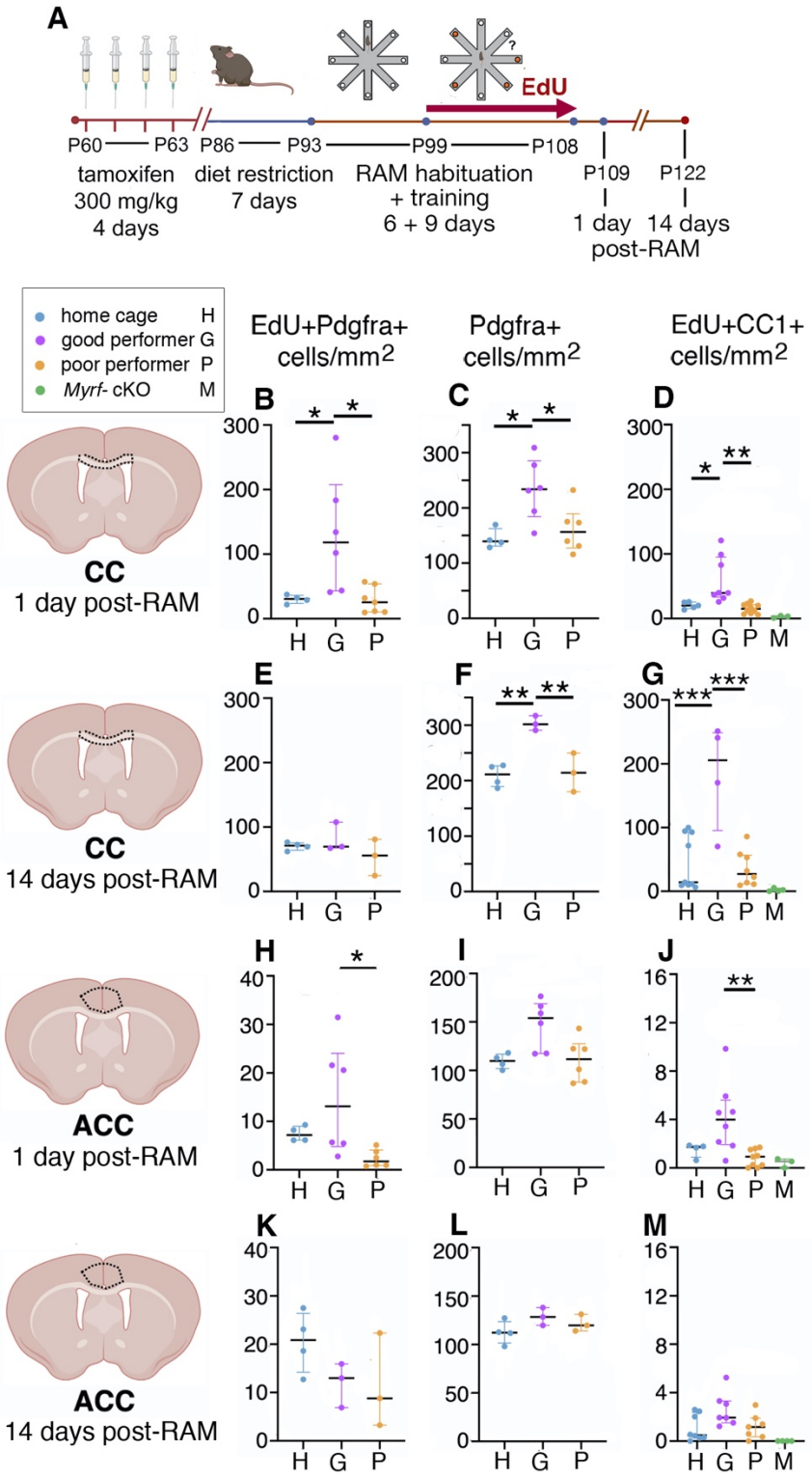

Figure 3. Successful working memory training stimulates proliferation and differentiation of OLPs. (**A**) Experimental protocol. Mice were given EdU in their drinking water during radial arm maze (RAM) training and perfusion-fixed 1- or 14-days post-training. RAM-trained mice were characterized as good- or poor-performers based on whether they achieved ≥10 or ≤5 "perfect trials", respectively, over the 9 days of RAM training. Home cage controls were not exposed to the

RAM at any time. (**B**-**D**) In the corpus callosum (CC) at 1-day post-RAM, the number-densities of proliferating OLPs (EdU^+ $Pdgfra^+$), all OLPs ($Pdgfra^+$) and newly-formed OLs (EdU^+CC1^+) were all increased in good-performers relative to poor-performers. Note that in the best of the good-performers nearly all OLPs proliferated (compare **B**,**C**). Poor-performers were indistinguishable from home cage controls. (**E**-**G**) In the CC at 14-days post-RAM densities of OLPs and newly-formed OLs were still elevated in good- versus poor-performers. The number of newly-differentiated OLs was increased further from 1-day post-RAM because of continuing OLP differentiation post-RAM (compare **D**,**G**). (**H**-**J**) Also in the anterior cingulate cortex (ACC) at 1-day post-RAM proliferating OLPs ($EdU^+Pdgfra^+$), all OLPs ($Pdgfra^+$) and newly-formed OLs (EdU^+CC1^+) were all more numerous in good- versus poor-performers, but by 14-days post-RAM all had returned to baseline (**K**-**M**). See Supplementary Table 1 for statistics. Similar data were also obtained for prelimbic/ infralimbic cortex, hippocampal CA1 and fimbria (Supplementary Fig. S3 and Supplementary Table 2). This figure includes data for *Myrf*-cKO mice (**D**, **G**, **J**, **M**), as a technical control for the experiments in Fig. 1. As expected, almost no new EdU^+CC1^+ OLs were produced in the *Myrf*-KOs. The *Myrf*-cKO dataset was not included in the statistical analysis.

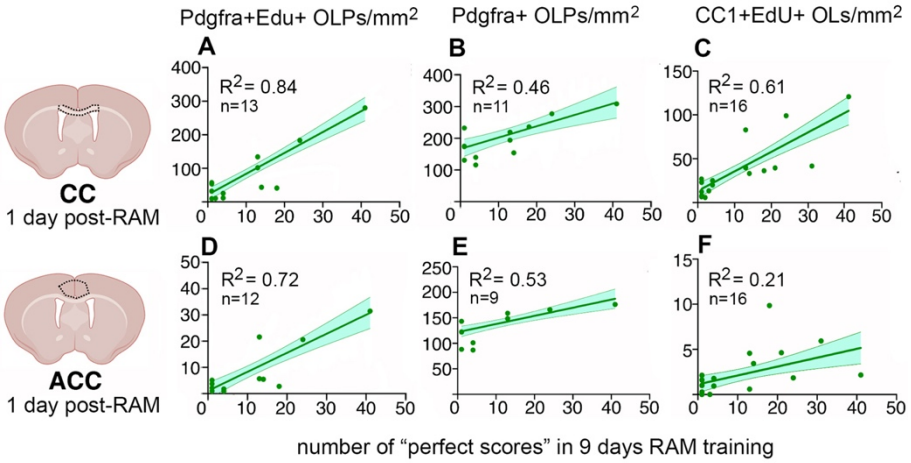

Figure 4. Working memory performance correlates with training-induced OLP proliferation and differentiation in individual mice. The working memory performance of individual mice in the radial arm maze (estimated by number of "perfect scores" during the 9 days of RAM training) correlates closely (R^2 >0.6) with the number-density of proliferating OLPs ($Pdgfra^+EdU^+$) counted on 1-day post-training in either their corpus callosum (CC) (**A**) or anterior cingulate cortex (ACC) (**D**), and with the density of newly-generated OLs ($CC1^+$ EdU^+) in the CC (**C**). Significant correlations (R^2 ~ 0.5) were also observed between performance and OLP population densities (**B**, **E**). Lines of best fit (simple linear regression) are drawn with 95% confidence intervals; R^2 and n values are shown on graphs and in Supplementary Table 3, together with slopes and intercepts. Corresponding data for prelimbic/infralimbic cortex, hippocampal CA1 and fimbria are shown in Supplementary Fig. S4 and Supplementary Table 3.

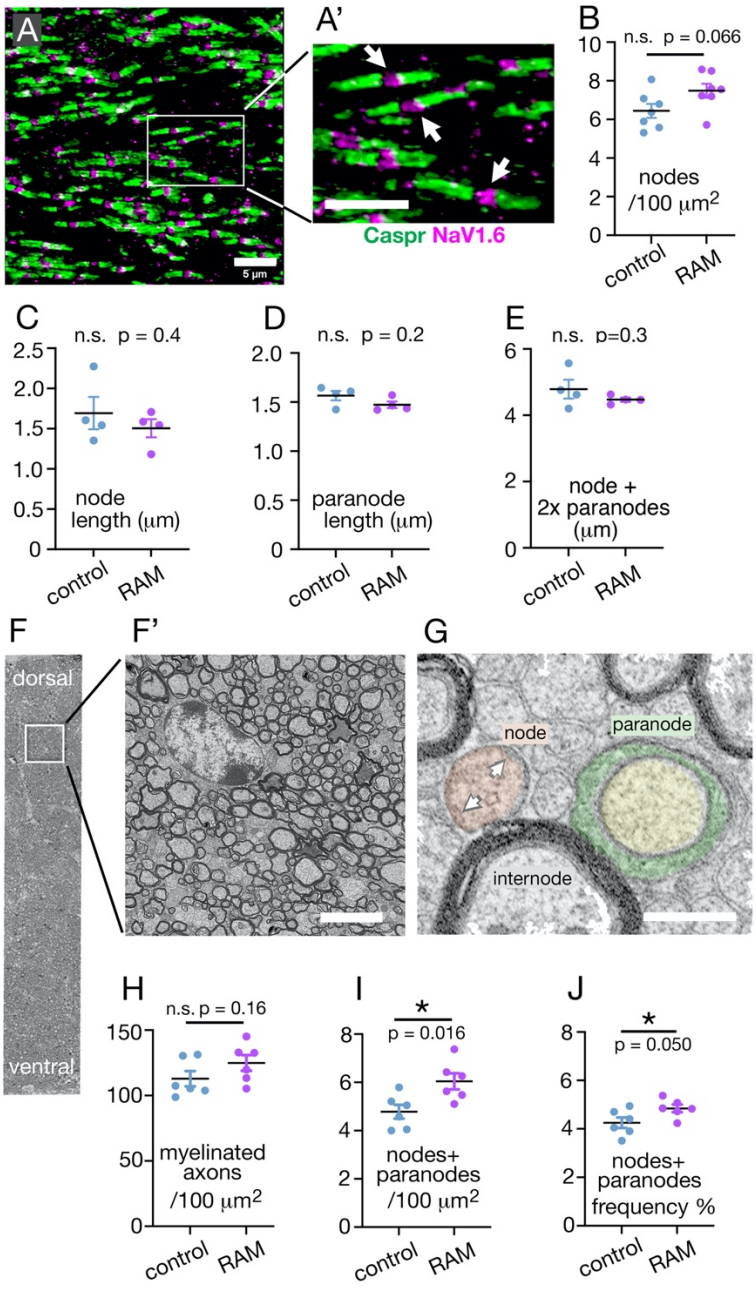

Figure 5. **Working memory training stimulates new myelin sheath production.**

(**A**) Confocal images of coronal sections through anterior corpus callosum (CC) at the level of the anterior cingulate cortex (ACC) were immunolabelled for $Na_V1.6$ (magenta) and Caspr (green) to visualize nodes and paranodes respectively. (**A'**) is a higher-magnification view of the area indicated in (**A**); *arrows* indicate nodes of Ranvier. (**B**) Node/paranode structures were counted in photographic images of 5 µm confocal stacks; there is a trend towards higher node/paranode density in good-performing RAM-trained mice compared to home-cage controls. (**C**-**E**) We measured the lengths of mature nodes of Ranvier as in Arancibia-Cárcamo et al. (2017) (see Methods). The mean lengths of nodes (**C**), paranodes (**D**) and complete nodal structures (node flanked by two paranodes, **E**) were not changed by RAM training. (**F**) Part of a wide-field EM

backscatter image (parasagittal), including the entire dorsal-ventral extent of the CC, 600 μm from its anterior tip; (**F'**) is a higher-magnification image of the area indicated in (**F**). (**G**) EM profiles of myelinated fibres sectioned through a node (false-colour orange), a paranode (false-colour green/yellow) and a myelin internode. Nodes can be distinguished from unmyelinated axons by the presence of electron-dense material undercoating the axonal membrane (*arrows*). All myelin internode (M), node (N) and paranode (P) profiles were counted in single ~ 260 x 50 μm areas of 100 nm thick sections such as (**F**) for each individual RAM-trained or home-cage control mouse (n=6 of each). (**H**) There was no significant change in myelinated axon (M+N+P) density in RAM-trained versus control mice, but a significant increase in the combined N+P density (**I**) and a marginally significant increase in the ratio (N+P)/(M+N+P) ("nodes + paranodes frequency") (**J**). Together these data indicate that there are more nodal structures, hence more internodes in RAM-trained versus control mice and suggest that those extra internodes might be shorter than the majority, consistent with their being recently-formed. *Scale bars:* **A**-**A',** 5 μm; **F'**, 5 μm; **G**, 2 μm

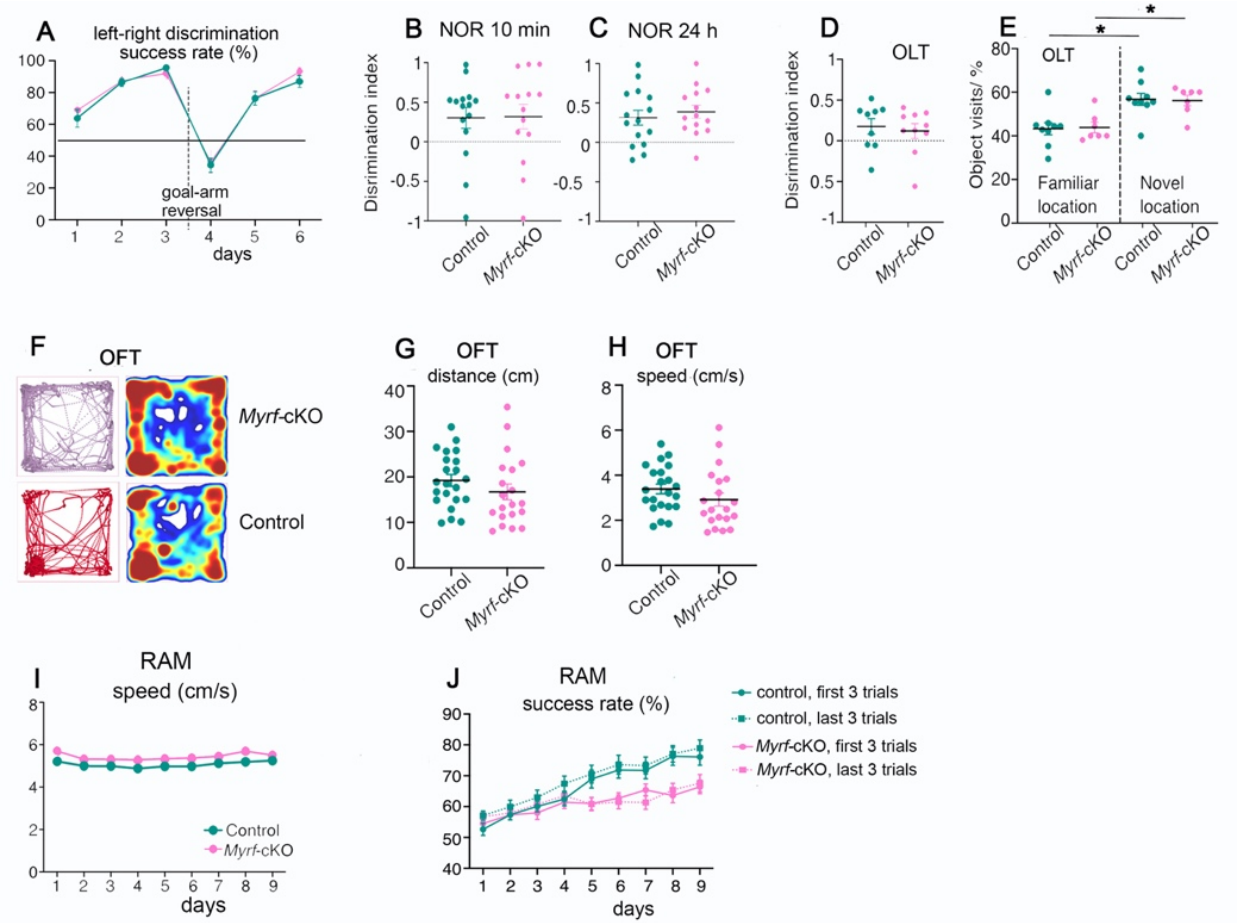

Supplementary Figure S1. **Behaviour of *Myrf*-cKO mice.** (**A**) *Myrf*-cKO (n=12) and control mice (n=16) performed indistinguishably in a T-maze left-right discrimination task, both before and after reversal of the goal-arm, demonstrating normal reference memory formation and reversal learning in the absence of new OL generation (repeated measures 2-way ANOVA time x genotype p=0.85, F (5, 130) = 0.39; time p<0.0001, F (5, 130) = 52.4; genotype p=0.38, F (1, 26) = 0.78; Šídák's multiple comparisons test did not detect any significant differences). (**B**, **C**) There was no difference between *Myrf*-cKO (n=14) and controls (n=15) in the novel object recognition (NOR) discrimination index after either 10 min delay (*Myrf*-cKO, 0.32 ± 0.15; control, 0.30 ± 0.13) (**B**) or 24 h delay (*Myrf*-cKO, 0.39 ± 0.082; control, 0.31 ± 0.094) (**C**) (Kolmogorov-Smirnov non-parametric test, p=0.3 at 10 min, D=0.37, p=0.7 at 24 h, D=0.26). (**D**, **E**) There was no difference between groups in the novel object location (NOL) task measured either by discrimination index (**D**) (*Myrf*-cKO, 0.12 ± 0.090, n=9; control, 0.18 ± 0.095, n=10, p=0.68, t=0.4, df=17) (unpaired Student's 2-tailed t-test) or frequency of visits to familiar or novel object locations (**E**) (familiar location: *Myrf*-cKO 43.8 ± 2.4%; control, 43.3 ± 2.8%. novel location: *Myrf*-cKO, 56.2 ± 2.4%; control, 56.8 ± 2.8%) (one-way ANOVA, F=8, df=28). Both *Myrf*-cKO and control groups visited the novel object location more frequently than the familiar object location [p=0.034 for control (familiar) vs control (novel); p=0.019 for *Myrf*-cKO (familiar) vs *Myrf*-cKO (novel)] (one-way ANOVA). (**F**-**H**) In the open field test (OFT), no obvious difference in the behaviour of *Myrf*-cKO

(n=21) versus control (n=22) groups was evident in bird's nest maps (left) or heat maps (right) (**F**). In the open field test there were also no differences between groups either in distance travelled (**G**) (*Myrf*-cKO, 16.7 ± 1.7 cm; control, 19.3 ± 1.3 cm, p=0.24, t=1.2, df=40), or running speed (**H**) (*Myrf*-cKO, 2.9 ± 0.29 cm/s; control, 3.4 ± 0.22 cm/s, p=0.20, t=1.3, df=40) (unpaired Student's 2-tailed t-tests). (**I**) In the radial arm maze (RAM), the average running speeds of *Myrf*-cKO and control mice were not significantly different over the 9 days of testing (repeated measures 2-way ANOVA, time x genotype F(8, 376) = 3.7, time F(5.5, 256) = 35, genotype F(1, 47) = 0.089, Šídák's multiple comparisons test).. (**J**) Success rates in the RAM task separated into the first 3 and last 3 of the 6 trials of each day showed no inter-trial differences between *Myrf*-cKO (n=28) and control (n=29) groups (repeated measures 2-way ANOVA, time x genotype F(24, 880) = 3.5, time F(5.8, 635) = 50, genotype F(3, 110) = 5.1, Tukey's multiple comparisons test), indicating that the reason *Myrf*-cKO mice performed less well than controls was not because of increased interference – they did not confuse arm visits made in later trials with those made in earlier trials.

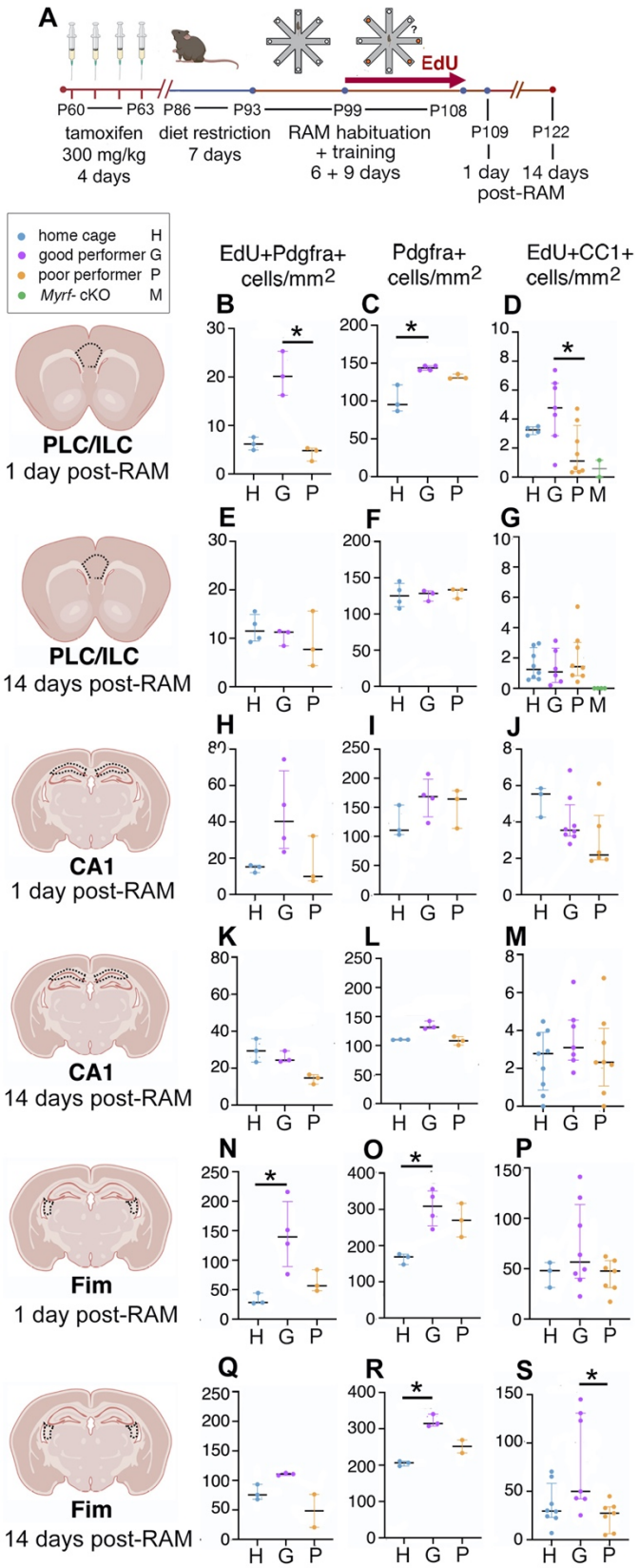

Supplementary Figure S2. Proliferation and differentiation of OLPs in good- versus poor-performers. (**A**) Experimental protocol. Mice were given EdU in their drinking water during radial arm maze (RAM) training and perfusion-fixed 1- or 14-days post-training. RAM-trained mice were

characterized as good- or poor-performers based on whether they achieved ≥10 or ≤5 "perfect trials", respectively, over the 9 days of RAM training. Home cage controls were not exposed to the RAM at any time. (**B**-**D**) In the prelimbic/ infralimbic cortex (PLC/ ILC at 1-day post-RAM, the number-densities of proliferating OLPs (EdU^+ $Pdgfra^+$), and newly-formed OLs (EdU^+CC1^+) were increased in good-performers relative to poor-performers, similar to anterior cingulate cortex (ACC, main text and Fig. 3). (**E**-**G**) By 14-days post-RAM, number densities of OL lineage cells had returned to pre-training (home cage control) levels, also like ACC. (**H**-**M**) In hippocampal CA1 there were no significant changes in the densities of OL lineage cells at 1-day (**H**-**J**) or 14-days post-RAM (**K**-**M**), although there was perhaps a trend towards increased density of EdU^+ $Pdgfra^+$ recently divided OLPs in good-performers versus controls (**H**). (**N**-**S**) In the Fimbria (Fim), OL dynamics were similar to the anterior corpus callosum (CC, main text and Fig. 3), but less pronounced. At 1-day post-RAM there was a shift towards a higher density of EdU^+ $Pdgfra^+$ recently-divided OLPs (**N**) and a parallel upwards shift in the density of EdU^+ $CC1^+$ newly-differentiated OLs (**P**) in good-performers versus both poor-performers or home-cage controls; however, only the increases over home cage controls reached statistical significance. By 14-days post-RAM the density of EdU^+ $Pdgfra^+$ OLPs had returned close to control levels while the increased density of EdU^+CC1^+ OLs in good-performers versus controls persisted. See Supplementary Table 2 for statistics.

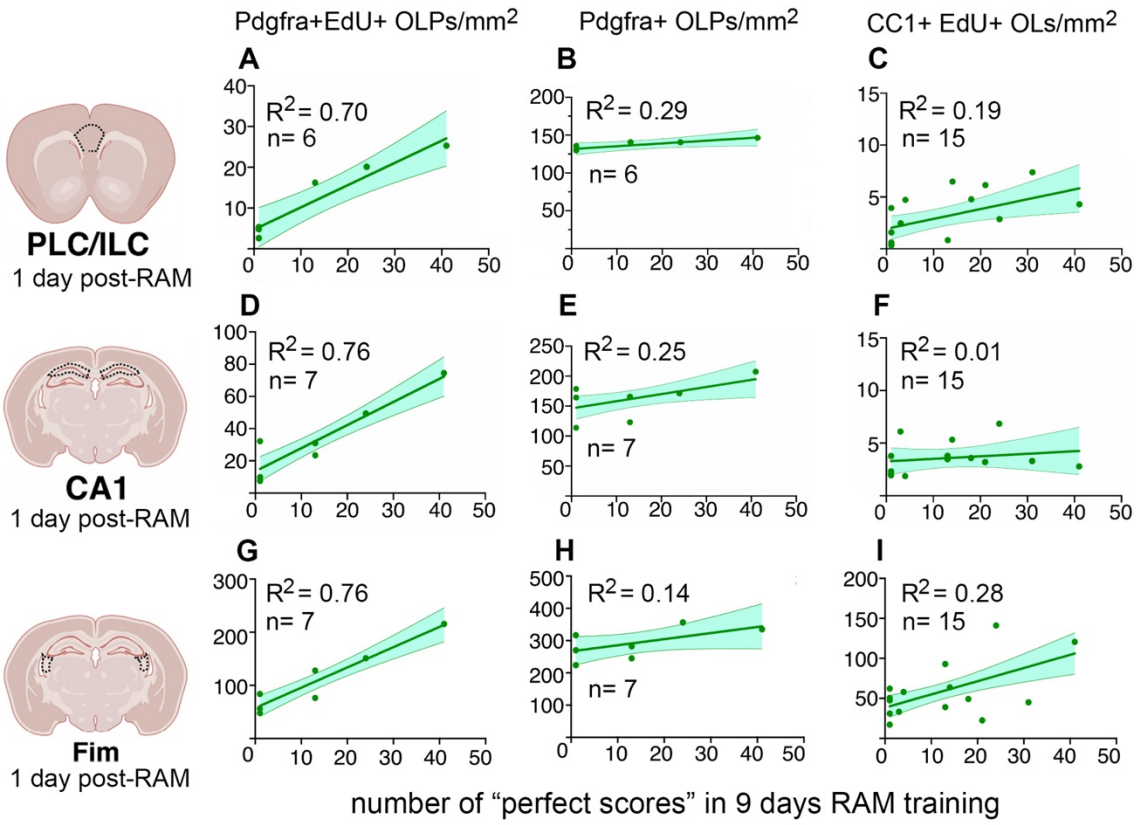

Supplementary Figure S3. Working memory score correlates with training-induced OLP proliferation and differentiation. At one day post-training, the working memory performance of individual mice in the radial arm maze (estimated by number of "perfect scores" during the 9 days of RAM training) correlates closely ($R^2 > 0.7$) with the number-density of proliferating OLPs ($Pdgfra^+$ EdU^+) in the prelimbic/infralimbic cortex (PLC/ILC, **A**) hippocampal CA1 (**D**) and fimbria (Fim, **G**) — but less so with the densities of newly-generated OLs ($CC1^+$ EdU^+) (**C**, **F**, **I**). Lines of best fit (simple linear regression) are drawn with 95% confidence intervals; R^2 and n values are shown on graphs and in Supplementary Table 3, together with slopes and intercepts.

	EdU$^+$ Pdgfra$^+$ OLPs	**Pdgfra$^+$ OLPs**	**EdU$^+$ CC1$^+$ OLs**
CC 1-day post-RAM Kruskal-Wallis test	H=8.5, p=0.007	H=7.1, p=0.02	H=14.7, p=0.0006
good	118 (43-208), n=6	234 (184-285), n=6	40 (33-95), n=8
poor	26 (11-54), n=7 p=0.006, q=0.006	157 (127-189), n=6 p=0.04, q=0.04	15 (8-22), n=10 p=0.0002, q=0.0002
home cage	31 (24-36), n=6 p=0.03, q=0.02	140 (131-163), n=4 p=0.02, q=0.03	20 (15-26), n=6 p=0.01, q=0.02
	EdU$^+$ Pdgfra$^+$ OLPs	**Pdgfra$^+$ OLPs**	**EdU$^+$ CC1$^+$ OLs**
CC 14-days post-RAM Kruskal-Wallis test	n.s. H=1.2, p=0.6	n.s. H=5.7, p=0.51	H=6.8, p=0.03
good	70 (68-108), n=3	302 (291-317) n=3	206 (95-249), n=4
poor	56 (25-81), n=3 n.s. p=0.3, q=0.7	214 (180-250), n=3 p=0.04, q=0.07	27 (12-57), n=8 p=0.02, q=0.01
home cage	71 (64-75), n=4 n.s. p=0.7, q=0.7	211 (189-227), n=4 p=0.03, q=0.07	14 (10-94), n=9 p=0.02, q=0.01
	EdU$^+$ Pdgfra$^+$ OLPs	**Pdgfra$^+$ OLPs**	**EdU$^+$ CC1$^+$ OLs**
ACC 1-day post-RAM Kruskal-Wallis test	H=9.2, p=0.003	H=5.8, p=0.047	H=11.1, p=0.001
good	13 (5-24), n=6	154 (118-169), n=6	4 (2-6), n=8
poor	2 (1-4), n=6 p=0.008, q=0.007	112 (88-128), n=6 p=0.045, q=0.07	0.9 (0.1-1.6), n=9 p=0.0009, q=0.002
home cage	7 (6-9), n=4 n.s. p=0.9, q=0.3	110 (102-117), n=4 p=0.04, q=0.07	1.7 (0.9-1.8), n=4 n.s. p=0.2, q=0.1
	EdU$^+$ Pdgfra$^+$ OLPs	**Pdgfra$^+$ OLPs**	**EdU$^+$ CC1$^+$ OLs**
ACC 14-days post-RAM Kruskal-Wallis test	n.s. H=2.9 p=0.3	n.s. H=4.3 p=0.1	n.s. H=5.6, p=0.056
good	13 (7-16), n=3	128 (120-138), n=3	1.9 (1.5-3.3), n=7
poor	9 (3-22), n=3 n.s. p=0.9, q=0.9	120 (114-131), n=3 n.s. p=0.4, q=0.4	1.2 (0.4-1.9), n=7 p=0.051, q=0.08
home cage	21 (14-26), n=4 n.s. p=0.2, q=0.3	112 (102-124), n=4 n.s. p=0.04, q=0.1	0.5 (0.3-2.4), n=8 p=0.03, q=0.08

Supplementary Table 1 Number-densities of OL lineage cells (cells/mm^2) following RAM training, comparing good-performers to poor-performers and home cage controls (median with interquartile range 25%-75%). Tabulated p-values refer to comparison with good-performers (Kruskal-Wallis

non-parametric test with Benjamini-Krieger-Yekutieli (BKY) correction for multiple comparisons). Uncorrected p-values are denoted “p” and corrected p-values as “q”. p-values > 0.05 are regarded as non-significant (n.s.). This table relates to Fig. 3.

	EdU$^+$ Pdgfra$^+$ OLPs	**Pdgfra$^+$ OLPs**	**EdU$^+$ CC1$^+$ OLs**
PLC/ILC 1-day post-RAM			
Kruskal-Wallis test	H=6.5, p=0.01	H=8.0, p=0.001	H=6.6, p=0.03
good	20 (16-25), n=3	144 (141-147), n=4	5 (3-7), n=7
poor	4.8 (2.6-5.3), n=3 p=0.01, q=0.02	130 (130-136) n=3 n.s. p=0.1, q=0.1	1.1 (0.4-3.6), n=8 p=0.01, q=0.02
home cage	6 (5-8), n=3 n.s. p=0.1, q=0.1	95 (87-121), n=3 p=0.005, q=0.01	3.3 (2.9-3.5), n=4 n.s. p=0.3, q=0.2
	EdU$^+$ Pdgfra$^+$ OLPs	**Pdgfra$^+$ OLPs**	**EdU$^+$ CC1$^+$ OLs**
PLC/ILC 14-days post-RAM			
Kruskal-Wallis test	n.s. H=0.89, p=0.7	n.s. H=1.1, p=0.6	n.s. H=0.69, p=0.7
good	11.3 (8.4-11.5), n=3	128 (118-132), n=3	1.1 (0.4-2.6), n=6
poor	8 (4-16), n=3 n.s. p=0.7, q=0.7	134 (121-134), n=3 n.s. p=0.4, q=0.6	1.4 (0.8-3.0), n=8 n.s. p=0.4, q=0.8
home cage	12 (9-15), n=4 n.s. p=0.6, q=0.7	125 (110-142), n=4 n.s. p=0.9, q=0.9	1.3 (0.6-2.7), n=8 n.s. p=0.7, q=0.8
	EdU$^+$ Pdgfra$^+$ OLPs	**Pdgfra$^+$ OLPs**	**EdU$^+$ CC1$^+$ OLs**
CA1 1-day post-RAM			
Kruskal-Wallis test	n.s. H=4.6, p=0.1	n.s. H=4.0, p=0.1	n.s. H=4.8, p=0.09
good	40 (25-68), n=4	1681 (34-198), n=4	4 (3-5), n=8
poor	10 (8-32), n=3 n.s. p=0.06, q=0.1	164 (114-179), n=3 n.s. p=0.6, q=0.6	2.2 (1.9-4.4), n=6 n.s. p=0.2, q=0.2
home cage	15 (12-16), n=3 n.s. p=0.08, q=0.1	111 (103-154), n=3 n.s. p=0.47, q=0.2	5.5 (4.3-5.9), n=3 n.s. p=0.2, q=0.2
	EdU$^+$ Pdgfra$^+$ OLPs	**Pdgfra$^+$ OLPs**	**EdU$^+$ CC1$^+$ OLs**
CA1 14-days post-RAM			
Kruskal-Wallis test	H=5.6, p=0.050	H=5.6, p=0.050	n.s. H=1.7, p=0.4
good	24.4 (23.7-29.4), n=3	132 (129-142), n=3	3.1 (2.4-4.6), n=7
poor	15 (11-17), n=3 n.s. p=0.07, q=0.1	108 (101-116), n=3 p=0.03, q=0.08	2.3 (1.1-4.1), n=8 n.s. p=0.3, q=0.5
home cage	29 (23-36), n=3 n.s. p=0.7, q=0.7	110 (110-111), n=3 n.s. p=0.08, q=0.1	2.8 (0.9-3.9), n=9 n.s. p=0.2, q=0.5
	EdU$^+$ Pdgfra$^+$ OLPs	**Pdgfra$^+$ OLPs**	**EdU$^+$ CC1$^+$ OLs**
Fim 1-day post-RAM			
Kruskal-Wallis test	H=7.3, p=0.005	H=6.3, p=0.02	n.s. H=1.8, p=0.4
good	140 (89-200), n=4	309 (255-351), n=4	57 (41-114), n=8

poor	57 (48-84), n=3 n.s. p=0.2, q=0.2	270 (224-317), n=3 n.s. p=0.5, q=0.3	48 (31-58), n=7 n.s. p=0.2, q=0.6
home cage	28 (27-44), n=3 p=0.007, q=0.02	169 (48-177), n=3 p=0.01, q=0.03	48 (31-56), n=3 n.s. p=0.4, q=0.6
	EdU$^+$ Pdgfra$^+$ OLPs	**Pdgfra$^+$ OLPs**	**EdU$^+$ CC1$^+$ OLs**
Fim 14-days post-RAM Kruskal-Wallis test	 n.s. H=5.1, p=0.06	 H=6.3, p=0.01	 H=6.8, p=0.03
good	111 (108-113), n=3	315 (308-341), n=3	50 (42-131), n=7
poor	49 (21-76), n=2 — — — —	252 (234-269), n=2 — — — —	28 (6-34), n=7 p=0.01, q=0.03
home cage	76 (68-93), n=3 n.s. p=0.07, q=0.1	207 (197-211), n=3 p=0.01, q=0.03	30 (23-58), n=8 n.s. p=0.06, q=0.06

Supplementary Table 2 Number-densities of OL lineage cells (cells/mm^2) following RAM training, comparing good-performers to poor-performers and home cage controls (median with interquartile range 25%-75%). Tabulated p-values refer to comparison with good-performers (Kruskal-Wallis non-parametric test with Benjamini-Krieger-Yekutieli (BKY) correction for multiple comparisons). Uncorrected p-values are denoted “p” and corrected p-values as “q”. p-values > 0.05 are regarded as non-significant (n.s.). Dashed lines indicate that small “n” precludes statistical analysis. This table relates to Supplementary Fig. S2.

	EdU^+ $Pdgfra^+$ OLPs	**$Pdgfra^+$ OLPs**	**EdU^+ $CC1^+$ OLs**
CC 1-day post-RAM			
R^2	0.84, n=12	0.46, n=11	0.61, n=18
Line of best fit (Y = mX + c)	Y = 6.3X + 21	Y = 3.6X + 169	Y = 2.2X + 13
Gradient significantly different from zero?	yes (p<0.0001)	yes (p<0.0001)	yes (p<0.0001)
ACC 1-day post-RAM			
R^2	0.64, n=10	0.53, n=10	0.21, n=17
Line of best fit	Y = 0.73X + 1	Y = 1.6X + 122	Y = 0.098X + 1
Gradient significantly different from zero?	yes (p<0.0001)	yes (p<0.0001)	yes (p=0.001)
PLC/ILC 1-day post-RAM			
R^2	0.70, n=6	0.29, n=6	0.19, n=15
Line of best fit	Y = 0.55X + 5	Y = 0.37X + 132	Y = 0.095X + 2
Gradient significantly different from zero?	yes (p=0.0002)	yes (p=0.046)	yes (p=0.0096)
CA1 1-day post-RAM			
R^2	0.76, n=7	0.25, n=7	0.010, n=15
Line of best fit	Y = 1.4X + 14	Y = 1.2X + 146	Y = 0.024X + 3
Gradient significantly different from zero?	yes (p=0.024)	yes (p<0.0001)	no (p=0.52)
Fim 1-day post-RAM			
R^2	0.76, n=7	0.14, n=7	0.28, n=15
Line of best fit	Y = 3.8X + 58	Y = 1.9X + 267	Y = 1.7X + 39
Gradient significantly different from zero?	yes (p<0.0001)	no (p=0.10)	yes (p=0.0002)

Supplementary Table 3 Lines of best fit (simple linear regression, Y=mX+c, where m is the slope and c the Y-intercept) and associated R^2 values, when number-densities of OL lineage cells (cells/mm^{-2}) are plotted against numbers of perfect trials attained by individual mice during RAM working memory training (Fig. 4 and Supplementary Fig. S4). P-values are not corrected for multiple comparisons, since they evaluate only whether or not the gradient of the line is different from zero.

Supplementary Video 1 A control mouse on days 1 and 8 of the T-maze rewarded alternation task.

Supplementary Video 2 A good-performing mouse on days 1 and 9 of the RAM task.

Supplementary Video 3 A poor-performing mouse on days 1 and 9 of the RAM task.

Supplementary Video 4 An *Myrf*-cKO mouse on days 1 and 9 of the RAM task.